

A global analysis of the SMEFT under the minimal MFV assumption

Riccardo Bartocci, Anke Biekötter, Tobias Hurth

PRISMA+ Cluster of Excellence & Institute of Physics (THEP) & Mainz Institute for Theoretical Physics, Johannes Gutenberg University, D-55099 Mainz, Germany

ABSTRACT: We present comprehensive global fits of the SMEFT under the *minimal* minimal flavour violation (MFV) hypothesis, i.e. assuming that only the flavour-symmetric and CP-invariant operators are relevant at the high scale. The considered operator set is determined by theory rather than the used datasets. We establish global limits on these Wilson coefficients using leading order and next-to-leading order SMEFT predictions for electroweak precision observables, Higgs, top, flavour and dijet data as well as measurements from parity violation experiments and lepton scattering. Our investigations reveal an intriguing crosstalk among different observables, underscoring the importance of combining diverse observables from various energy scales in global SMEFT analyses.

Contents

1	Introduction	2
2	The $U(3)^5$ symmetric SMEFT	3
3	Datasets	4
3.1	Electroweak precision observables	5
3.2	Higgs and electroweak boson observables	5
3.3	Top observables	6
3.4	Parity violation experiments and lepton scattering	6
3.5	Drell-Yan observables	6
3.6	Flavour observables	7
3.7	Dijet+photon production	7
4	Global fit using leading order predictions	8
5	Global fit including next-to-leading order predictions	9
5.1	SMEFT predictions at NLO	10
5.2	Global fit	10
6	Interplay between the datasets	13
6.1	EWPO and PVE datasets	16
6.2	Drell-Yan, PVE and flavour datasets	17
6.3	Top, flavour and dijet datasets	19
7	Conclusions and outlook	20
A	Δ_{CKM} as an additional low-energy observable	22
B	Flavour symmetric and CP even operators	23
C	Observables	24
D	Numerical results	28
E	LEFT Hamiltonians for the relevant flavour observables	30

1 Introduction

The Standard Model (SM) of particle physics describes the interactions of fundamental particles with remarkable success. However, it fails to resolve some outstanding issues including the nature of dark matter, the origin of neutrino masses, and the electroweak hierarchy problem. In the absence of a direct discovery of new physics (NP), Standard Model Effective Field Theory (SMEFT) [1–4] enables us to systematically explore the low-energy effects of NP at currently inaccessible energy scales. SMEFT relies only on minimal assumptions and extends the dimension-four SM Lagrangian by higher-dimensional operators built from the SM fields and respecting the SM gauge symmetries.

The SMEFT framework has been extensively used to describe NP effects in experimental data and analyse the viable NP directions up to dimension six in global analyses. The selection of the Wilson-coefficient sets in these analyses has mostly been determined by the choice of the datasets and global analyses of low-energy [5], electroweak [6–10] and top [11–15] data as well as combinations thereof [16–18] have been performed. Nonetheless, global fits of all dimension-six SMEFT operators are (currently) intractable due to the enormous number of Wilson coefficients. The completely flavour-general SMEFT Lagrangian has 2499 free parameters, the so-called Wilson coefficients, at mass dimension six [19–21] (1350 of which are CP-even and 1149 are CP-odd). However, this number can be drastically reduced when considering specific flavour assumptions.

Since flavour observables push the appearance of flavour-violating operators far above the TeV scale [22, 23], it is natural to explore specific assumptions on flavour symmetries and their breaking pattern. These various symmetry assumptions lead to some model dependence and can be regarded as universality classes providing an organisation principle for the SMEFT, allowing to systematically analyse the pattern of NP [24, 25].

Contributions to flavour-violating observables can be suppressed under the assumption of minimal flavour violation (MFV), which allows the SM Yukawa couplings as the only sources of $U(3)^5$ breaking [26–28]. Previous works within the standard MFV scenario restrict the number of operators to those relevant to the respective datasets considered in these analyses, see e.g. [29–31]. In the analyses of [32, 33] the so-called leading MFV hypothesis was used which includes the additional assumption that the NP at the high scale does not include any flavour changing neutral currents (FCNC) at tree level. In all cases, the number of operators is finally determined by the considered datasets rather than by theory, as a global analysis of all NP directions in these scenarios is currently not possible¹.

In this work, we consider the *minimal* MFV scenario and assume an exact $U(3)^5$ flavour symmetry of NP operators at the high scale within the MFV hypothesis. This assumption reduces the total number of Wilson coefficients to 47 at the high scale. Six of these coefficients correspond to CP-odd operators, which typically require dedicated observables to constrain them and therefore only have a minimal crosstalk with CP-even operators in global analyses [36], see e.g. [37–47] for dedicated analyses of CP-odd operators. We therefore set these contributions aside and consider a set of 41 (CP even) Wilson

¹Setting only single-parameter limits on the Wilson coefficients in models under different flavour assumptions allows to set limits on the general NP scale of such models, see e.g. recent analyses [34, 35].

coefficients in total ². We denote this assumption the *minimal* MFV hypothesis because it corresponds to creating the minimal amount of flavour violation at the electroweak scale. In contrast to the MFV hypothesis, the exact $U(3)^5$ flavour symmetry assumed at the NP scale is not a renormalisation group invariant concept.

Our analysis confronts the Wilson coefficients of the minimal MFV SMEFT with data from electroweak precision observables (EWPO), low-energy parity violation experiments, as well as Higgs, top, flavour, Drell-Yan (DY) and dijet data. These datasets enable us to perform a complete global fit within the minimal MFV hypothesis, testing a parameter set which is motivated by theory rather than data. We identify which datasets set the strongest bounds on each operator and analyse the crosstalk between different datasets in a global fit. For example, we will analyse the roles of Drell-Yan data as well as parity violation observables for constraining semileptonic operators and the interplay of top, flavour and dijet observables for constraining four-quark operators. Our main goal is to investigate the ingredients needed to perform a global fit of the SMEFT in which all the directions in parameter space are reasonably constrained. We will show that in order to significantly constrain all 41 Wilson coefficients of the minimal MFV SMEFT, we have to rely on partial next-to-leading order (NLO) SMEFT predictions as some four-quark operators are essentially unconstrained at leading order (LO). The additional degeneracies induced in the SMEFT predictions at NLO only marginally impact the global analysis given the current level of constraints from other datasets.

Our paper is organised as follows: In Section 2, we define the minimal MFV and introduce the notation. In Section 3, we describe the considered datasets and list the Wilson coefficients constrained by each set. We present global analyses using LO predictions only or including partial NLO predictions in Sections 4 and 5, respectively. In Section 6, we analyse the interplay between different datasets in the global fit. We conclude in Section 7.

2 The $U(3)^5$ symmetric SMEFT

The SMEFT Lagrangian, truncated at dimension six, is given by

$$\mathcal{L}_{\text{SMEFT}} = \mathcal{L}_{\text{SM}} + \sum_i \frac{C_i}{\Lambda^2} Q_i, \quad (2.1)$$

where C_i are the Wilson coefficients of the operators Q_i and Λ denotes the NP scale, which we set to $\Lambda = 4 \text{ TeV}$ throughout our work. We truncate all SMEFT predictions at linear order in the Wilson coefficients, neglecting quadratic contributions which are suppressed by Λ^{-4} and therefore formally of the same order as dimension-eight contributions. We employ $\{\alpha, M_Z, G_F\}$ as our electroweak input parameters.

Symmetries play a big role in the SM and beyond. The SM as well as the operators of SMEFT rely on Lorentz and gauge symmetries. A priori, there are no restrictions on

²Starting from the 59 flavour-universal operators of the Warsaw basis [3] one finds that only 42 of them (36 CP even + 6 CP odd) can be made flavour symmetric without an additional Yukawa coupling. For 5 of the 36 CP-even operators, there are two independent flavour-symmetric ways to contract the flavour indices, which leads to 47 operators in total (with 41 CP even and 6 CP odd ones).

the flavour structure in the SMEFT. However, the fact that explicit flavour violation is experimentally extremely constrained [22, 23] makes it natural to assume symmetries for the flavour sector. We work in the up-basis, where the SM CKM matrix is located in the down component of the quark doublets, and assume no flavour violation at the NP scale in the SMEFT. Equivalently, we consider a $U(3)^5$ symmetry of the SMEFT, namely

$$U(3)^5 = U(3)_\ell \times U(3)_q \times U(3)_e \times U(3)_u \times U(3)_d, \quad (2.2)$$

where $\{\ell, q, e, u, d\}$ represent the SM fermions [24]. The $U(3)^5$ symmetric SMEFT contains only the minimum and non-removable amount of flavour violation which results from the SM Yukawa couplings. Under this assumption, there are 47 independent SMEFT operators. Note that the contraction of the flavour indices of flavour-generic operators can result in two independent $U(3)^5$ singlets in some cases. This is the case for four-fermion operators with two fermion currents of the same chirality: $Q_{qq}^{(1)}$, $Q_{qq}^{(3)}$, Q_{ll} , Q_{dd} and Q_{uu} . For these operators, we hence introduce unprimed and primed Wilson coefficients which refer to the operators contracting the flavour indices within the fermion bilinears or between the two different fermion bilinears, respectively. As an example, the operator $Q_{ll} = (\bar{l}_i \gamma_\mu l_j)(\bar{l}_k \gamma^\mu l_l)$ has two flavour-symmetric contractions

$$C_{ll} \delta_{ij} \delta_{lk} \quad \text{and} \quad C'_{ll} \delta_{ik} \delta_{jl}. \quad (2.3)$$

For the operator Q_{ee} , a Fierz identity implies a single independent coefficient C_{ee} . Limits on the primed and unprimed Wilson coefficients can generally be different. As an example, C'_{ll} enters the shift of the Higgs vacuum expectation value to leave the input parameter G_F unchanged and is therefore tightly constrained through EWPO. C_{ll} , on the other hand, is dominantly constrained through $e^- e^+ \rightarrow l^- l^+$ observables and its limits are weaker than those on C'_{ll} .

Note that even though all operators of the $U(3)^5$ symmetric SMEFT are flavour conserving, flavour-violating effects still occur due to flavour violation in the SM. The renormalisation group (RG) evolution from the NP scale Λ down to the electroweak scale and below generates contributions to flavour-violating observables – via the interplay between the flavour-violating SM interactions and the flavour-conserving NP vertices. Therefore, even the operators of the $U(3)^5$ symmetric SMEFT can be constrained by flavour observables [32].

Six of the 47 $U(3)^5$ symmetric operators are (purely bosonic and) CP odd and are best constrained through dedicated CP-sensitive observables and have negligible crosstalk with CP even operators [37]. Therefore, we set them aside in our analysis. We list the 41 CP even operators considered in our analysis in Table 2 in appendix B.

3 Datasets

In our analysis, we include data from EWPO, Higgs, top, low-energy parity violation experiments (PVE), lepton scattering, flavour, Drell-Yan as well as dijet+photon production. We list the corresponding observables and operator sets constrained in each dataset in the following. A graphical representation of operator sets contributing to the different observables is shown in Figure 1.

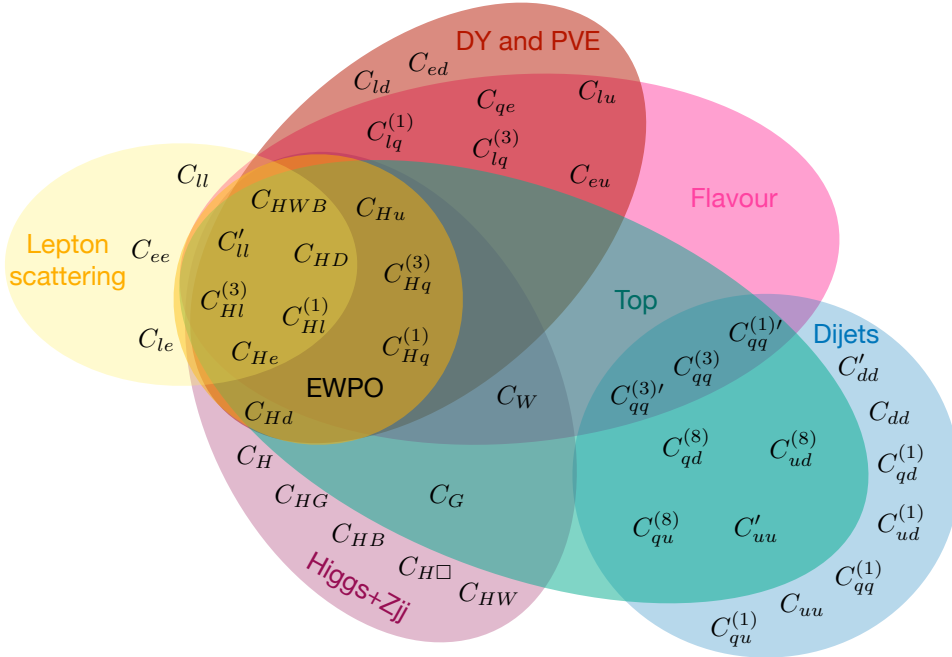


Figure 1: Venn diagram showing the operator sets contributing to the individual datasets at LO.

3.1 Electroweak precision observables

We utilise a total of 13 electroweak precision observables, including pseudo-measurements on the Z resonance [48], a combination of the W mass measurements at LEP [49], Tevatron [50] and ATLAS [51] and the LEP and Tevatron combination of the decay width of the W boson [52]³

$$\Gamma_Z, \sigma_{\text{had}}^0, R_l^0, A_l, A_{FB}^l, R_c^0, A_c, A_{FB}^c, R_b^0, A_b, A_{FB}^{0,b}, m_W, \Gamma_W. \quad (3.1)$$

These measurements constrain the following operator set at leading order

$$\text{OS}_{\text{EWPO}} = \{C_{HWB}, C_{HD}, C_{Hl}^{(1)}, C_{Hl}^{(3)}, C_{Hq}^{(1)}, C_{Hq}^{(3)}, C_{Hu}, C_{Hd}, C_{He}, C_{Hl}'\}. \quad (3.2)$$

3.2 Higgs and electroweak boson observables

We include observables from the Higgs sector as included in [10]. These include Higgs signal-strength measurements for various production and decay channels, simplified tem-

³It was pointed out in [53–56] that combinations of the measurements of W -boson mass and its decay width can be problematic as both results are partially based on the same datasets. We have explicitly checked that removing Γ_W from our dataset does not influence our limits beyond the 5% level. Moreover, it was suggested that LEP data should in principle not enter the combined measurement of the W boson mass due to its extraction from W^+W^- production, which makes it sensitive to modified triple-gauge couplings [55, 56]. However, given that the ATLAS and Tevatron measurements dominate the combination, we expect the impact on our fit to be small.

plate cross section (STXS) measurements and differential distributions. SMEFT predictions for the Higgs decays are based on [57]. For di-Higgs production, we include signal-strength measurements in the $4b$, $2b2\tau$ and $2b2\gamma$ final states. Moreover, we consider the angular distribution $\Delta\phi_{jj}$ in Zjj production, which is known to dominantly constrain the Wilson coefficient C_W . The full list of observables is given in Table 3. The set of operators contributing to Higgs observables and Zjj production is given by

$$\text{OS}_{\text{EWPO}} + \{C_W, C_G, C_{HB}, C_{HW}, C_{HG}, C_H, C_{H\Box}\}. \quad (3.3)$$

3.3 Top observables

For the top sector, we reuse the datasets and corresponding predictions from fitmaker [16]. These include cross-section measurements, differential distributions and asymmetry observables for single-top, $t\bar{t}$ and ttV production. The observables are listed in Tables 4-5. The set of operators contributing to top observables is given by

$$\text{OS}_{\text{EWPO}} + \{C_W, C_G, C_{qq}^{(1)'}, C_{qq}^{(3)}, C_{qq}^{(3)'}, C'_{uu}, C_{ud}^{(8)}, C_{qu}^{(8)}, C_{qd}^{(8)}\}. \quad (3.4)$$

3.4 Parity violation experiments and lepton scattering

With the aim of constraining semileptonic operators, we include data from atomic parity violation (APV) and parity violating electron scattering (PVES) experiments, which we collectively refer to as parity violation experiments (PVE). Specifically, we include the weak charge Q_W of ^{133}Cs [58] and of the proton [59], deep inelastic scattering of polarised electrons as measured by the PVDIS experiment [60] and measurements of parity-violating scattering provided by SAMPLE [61].

As a constraint on purely leptonic operators, we use muon neutrino-electron scattering, the weak mixing angle measured in parity violating electron scattering [58], τ polarisation measured in $e^+e^- \rightarrow \tau^+\tau^-$ [62] as well as differential cross sections and asymmetries in $e^+e^- \rightarrow l^+l^-$ [49, 62, 63]. The corresponding theory predictions are taken from [5, 64]. The set of operators entering our low-energy observables is given by

$$\text{OS}_{\text{EWPO}} + \{C_{lq}^{(1)}, C_{lq}^{(3)}, C_{ed}, C_{eu}, C_{ld}, C_{lu}, C_{qe}, C_{ll}, C_{ee}, C_{le}\}. \quad (3.5)$$

3.5 Drell-Yan observables

Semileptonic operators can also be constrained in Drell-Yan lepton production. We use the *HighPT* [65] tool to obtain the theory predictions for differential distributions of the $pp \rightarrow ee, \mu\mu, \tau\tau$ processes at leading order in the SMEFT. The corresponding experimental datasets are listed in Table 5. To avoid conflicts with the EFT validity range, we only use invariant mass bins up to an energy of 3 TeV. We describe the differential Drell-Yan cross sections by the following set of operators

$$\text{OS}_{\text{EWPO}}(\text{without } C_{HWB}, C_{HD}, C'_{ll}) + \{C_{lq}^{(1)}, C_{lq}^{(3)}, C_{ed}, C_{eu}, C_{ld}, C_{lu}, C_{qe}\}. \quad (3.6)$$

Note that currently shifts of the SM parameters as a result of the scheme choice are not taken into account in *HighPT*. Consequently, the Wilson coefficients C_{HWB} , C'_{ll} and C_{HD} , which only contribute to the Drell-Yan dataset through these shifts, are not taken into account. Given that these coefficients are tightly constrained by EWPO, we expect the impact of the missing contributions to be subdominant.

3.6 Flavour observables

We utilise the datasets and predictions as implemented in *Flavio* [66–69] for flavour-sector observables. These include differential branching ratios of B mesons and Kaons, angular observables as well as the R_K and R_K^* ratios. A comprehensive list of the flavour observables included in our analysis is provided in Table 6. As these observables are defined at low energies, we study them in the so-called Low Energy Effective Field Theory (LEFT). We present the effective Hamiltonians for the relevant flavour observables in Appendix E. Starting from the Lagrangian definition in Equation (2.1), we perform the running from the high scale ($\mu = 4$ TeV) to the electroweak scale ($\mu = M_Z$), where we match the SMEFT onto the LEFT, using *DsixTools* [67–71]. For the subsequent running from the electroweak (EW) scale to the bottom-quark mass scale in the LEFT, we use the *Wilson* package [72]. As a cross check, we have explicitly confirmed that we can reproduce the results presented in [33]. The SMEFT Wilson coefficients appearing in the theory predictions of flavour violating processes are

$$\text{OSEWPO}(\text{without } C_{Hd}) + \{C_W, C_{lq}^{(1)}, C_{lq}^{(3)}, C_{lu}, C_{eu}, C_{qe}, C_{qq}^{(1)'}, C_{qq}^{(3)}, C_{qq}^{(3)'}\}. \quad (3.7)$$

3.7 Dijet+photon production

LHC dijet production provides an interesting probe of the 4-quark-operator parameter space. However, the trigger threshold for jets at the LHC restricts the testable kinematic region to dijet invariant masses to the multi-TeV range. At high energies, the quadratic terms of the EFT expansion often dominate over the linear ones, potentially leading to conflicts with the EFT validity [73]. Considering instead the production of two jets in association with a photon [74] enables us to probe lower dijet invariant-mass ranges $m_{jj} < 1.2$ TeV and circumvent this issue.

We have validated the SM dijet invariant-mass distribution of Figure 1 of [74] using *Madgraph* [75, 76] Monte Carlo data and implemented the relevant cuts in a *Rivet* [77] analysis for the event selection. We have excluded the region $m_{jj} < 500$ GeV, where we expect detector effects to be more relevant. Using a flat factor $\epsilon_{\text{det}} = 0.28$ for the experimental detector efficiency, we can reproduce the ATLAS SM distribution within 10%. Using SMEFTsim [78], we have determined the SMEFT prediction for each bin of the differential cross section at LO in SMEFT. The obtained predictions are available as an ancillary file with the arXiv submission.

It is worth noting that some of the considered four-quark operators, $Q_{qd}^{(1)}$, $Q_{qu}^{(1)}$, $Q_{ud}^{(1)}$, do not interfere with the dominant SM diagram, the t -channel exchange of a gluon. As a result, we expect the quadratic SMEFT contributions for these operators, which we generally neglect in our study, to be dominant with respect to their linear counterparts. To highlight this effect, we present the ratio for bounds from single-parameter fits based on linear SMEFT predictions only over bounds from linear+quadratic fits in Table 1. As anticipated, the limits on $C_{qd}^{(1)}$, $C_{qu}^{(1)}$, $C_{ud}^{(1)}$ are tightened by more than a factor 2.5 in a quadratic fit. Since we will only underestimate the limits on these Wilson coefficients in our linear fit, we will keep their linear contributions. The remaining operators are much more mildly influenced, typically by 10 – 20%, in a quadratic fit.

$C_{qq}^{(1)}$	$C_{qq}^{(1)prime}$	$C_{qq}^{(3)}$	$C_{qq}^{(3)prime}$	$C_{qd}^{(8)}$	$C_{qu}^{(8)}$	$C_{ud}^{(8)}$	C_{dd}	C_{dd}^{prime}	C_{uu}	C_{uu}^{prime}	$C_{qd}^{(1)}$	$C_{qu}^{(1)}$	$C_{ud}^{(1)}$	C_G
0.9	0.9	1.0	1.0	1.7	1.4	1.6	2.5	2.2	0.9	0.9	5.9	3.9	2.6	1.4

Table 1: Ratio of the 68% CL limits on the operators contributing to dijet+photon production at linear and quadratic order in SMEFT.

We neglect the clearly subdominant electroweak contributions to dijet production and describe the differential distributions by

$$\{C_G, C_{qd}^{(1)}, C_{qu}^{(1)}, C_{ud}^{(1)}, C_{qq}^{(1)}, C_{qq}^{(1)prime}, C_{qq}^{(3)}, C_{qq}^{(3)prime}, C_{uu}, C_{uu}^{prime}, C_{dd}, C_{dd}^{prime}, C_{ud}^{(8)}, C_{qu}^{(8)}, C_{qd}^{(8)}\}. \quad (3.8)$$

4 Global fit using leading order predictions

We perform a χ^2 analysis of the data \vec{d} with linear SMEFT predictions $\vec{p}(C_i)$ taking into account correlations in the covariance matrix V , where known. The χ^2 function is given by

$$\chi^2(C_i) = \left(\vec{d} - \vec{p}(C_i)\right)^T V^{-1} \left(\vec{d} - \vec{p}(C_i)\right). \quad (4.1)$$

For our global analyses, we obtain the limits on a Wilson coefficient while profiling over the remaining parameters using the toy Monte Carlo method.

We present our global analysis with SMEFT predictions at LO in Figure 2. Operators from the Higgs-EW sector as well as four-lepton operators, shown in the upper panel of the plot, are well constrained. All corresponding Wilson coefficients, except C_H , are constrained to a region within $|C|/\Lambda^2 < 1/\text{TeV}^2$ at 95% CL. The four-fermion operators involving quark fields, shown in the lower panel of the plot, are generally more weakly constrained. The limits of two of the seven semileptonic operators as well as nine of the 14 four-quark operators exceed $|C|/\Lambda^2 = 1/\text{TeV}^2$ (on at least one side). In particular, $C_{qd}^{(1)}$, $C_{ud}^{(1)}$, $C_{qu}^{(1)}$, C_{dd} and C_{dd}^{prime} are essentially unconstrained, with limits on $|C|/\Lambda^2$ greater than $50/\text{TeV}^2$. Nevertheless, it is interesting to note that the inclusion of these very weakly constrained operators does not invalidate the limits on the remaining Wilson coefficients.

All 41 Wilson coefficients included in our global fit are consistent with the SM within 2σ . However, six Wilson coefficients exhibit deviations exceeding 1.5σ

$$\{C_{ll}, C_{ee}, C_{lu}, C_{lq}^{(1)}, C_{qq}^{(1)}, C_{qq}^{(3)}\}. \quad (4.2)$$

The shift in C_{ll} can be attributed mainly to a small deviation in the measurement of the differential cross-section of $e^+e^- \rightarrow e^+e^-$, while C_{ee} is affected by the measurement of the weak mixing angle in parity-violating electron scattering (g_{AV}^{ee}). Several semileptonic operators exhibit deviations from the SM, with the largest shifts arising for C_{lu} and $C_{lq}^{(1)}$. These deviations are primarily induced by the Drell-Yan data, in particular with muons in the final state. In the four-quark sector, $C_{qq}^{(3)}$ is dominantly shifted by single-top production data and the shift of $C_{qq}^{(1)}$ is dominated by dijet data, which is the only observable constraining this operator at LO.

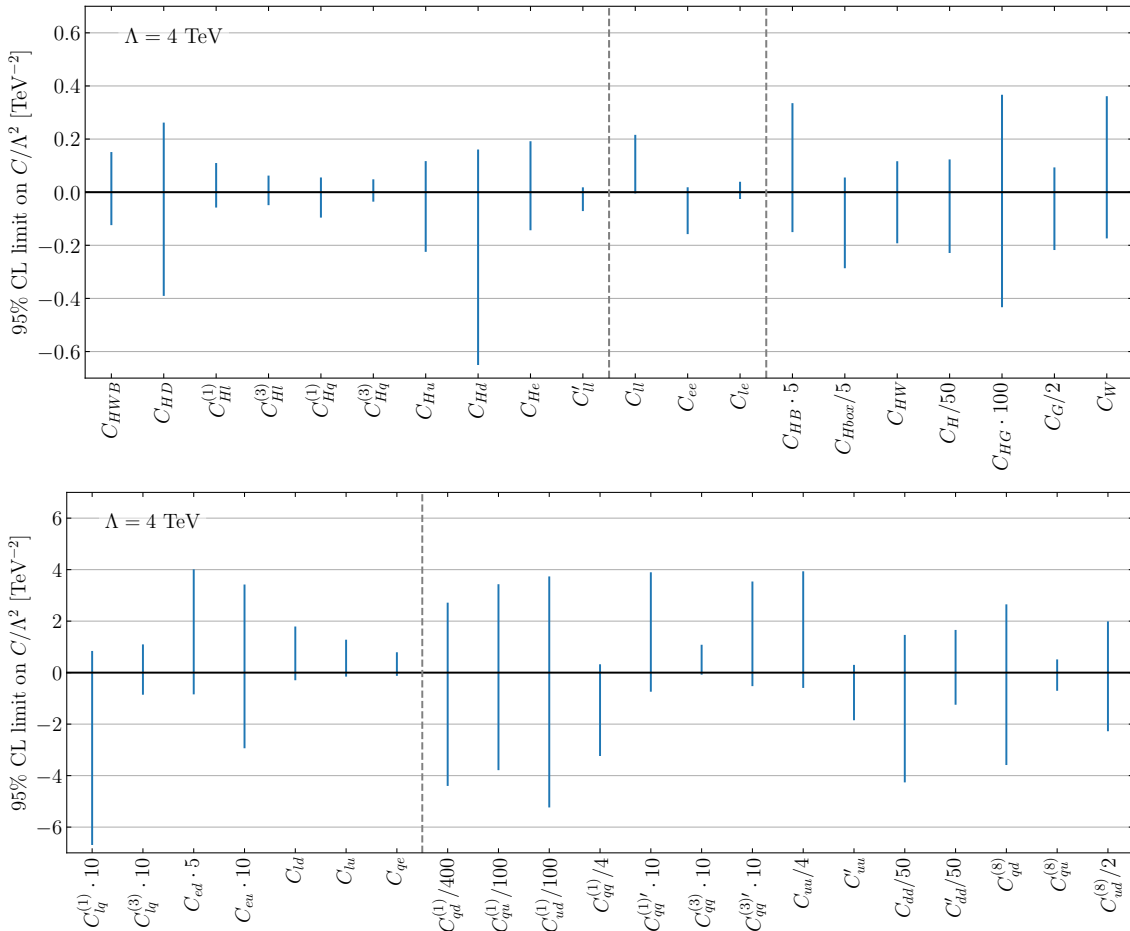


Figure 2: Limits on the Wilson coefficients in a global analysis using LO SMEFT predictions.

5 Global fit including next-to-leading order predictions

As shown in the previous section, some four-quark operators within the minimal MFV set remain weakly constrained in a leading-order fit to our datasets. These operators contribute to a number of precisely measured observables at NLO. In this section, we perform a global analysis based on NLO predictions, where present. This includes NLO predictions for EWPO [79, 80] as well as partial NLO predictions for $t\bar{t}$ production [81, 82] and Higgs decays to bottom quark pairs [83]. Note that not all observables are considered at NLO precision in our partial NLO global analysis. As a result, our analysis does not consider all degeneracies which might be present in the SMEFT predictions at NLO⁴. Nevertheless, the inclusion of EWPO at NLO precision serves as a good testcase to study the impact of the additional freedom in the Wilson coefficient space at NLO on the operators present already at LO.

⁴See e.g. [83] for an example of how the consideration of further NLO effects can spoil the loop sensitivity to the Higgs self-coupling.

5.1 SMEFT predictions at NLO

EWPO We include NLO predictions for EWPO from [79, 80], see also [84] for partial results in other EW input schemes. At NLO precision, EWPO are sensitive to 25 additional Wilson coefficients. Explicitly, the considered NLO EWPO predictions are sensitive to

$$\{C_{ll}, C_{ee}, C_{le}, C_{HB}, C_{H\Box}, C_{HW}, C_W, C_{lq}^{(1)}, C_{lq}^{(3)}, C_{ed}, C_{eu}, C_{ld}, C_{lu}, C_{qe}, C_{qd}^{(1)}, C_{qu}^{(1)}, C_{ud}^{(1)}, C_{qq}^{(1)}, C_{qq}^{(1)'}, C_{qq}^{(3)}, C_{qq}^{(3)'}, C_{uu}, C'_{uu}, C_{dd}, C'_{dd}\}, \quad (5.1)$$

in addition to those listed in Equation (3.2).

Top SMEFT predictions for top observables at NLO are provided by the SMEFit collaboration [81, 82], which employs the $\{G_F, M_W, M_Z\}$ input scheme. While this input scheme is different from the one utilised in our analysis, the impact of the electroweak input-scheme choice on top quark physics is expected to be small. We have explicitly checked that the LO predictions for m_{tt} differential distributions are very similar in the two input schemes. To improve the bounds on some four-quark operators, we update the predictions for the charge asymmetry as well as m_{tt} differential distributions to NLO precision as a proof-of-principle. These observables have been shown to have the largest constraining power for four-quark operators [82]. NLO predictions of the considered top quark production processes add sensitivity to the operators

$$\{C_{qd}^{(1)}, C_{qu}^{(1)}, C_{ud}^{(1)}, C_{qq}^{(1)}, C_{uu}\}. \quad (5.2)$$

Higgs The dominant contributions of third generation four-quark operators to single-Higgs production and decay are known [83]. We include the NLO predictions for gluon fusion Higgs production, $t\bar{t}h$ production and the loop-induced decays $h \rightarrow gg, \gamma\gamma$, which receive contributions from the operators

$$\{C_{qu}^{(1)}, C_{qq}^{(1)}, C_{qq}^{(3)}, C_{uu}, C_{qu}^{(8)}\}. \quad (5.3)$$

Specifically, $C_{qu}^{(1)}, C_{uu}, C_{qu}^{(8)}$ contribute to $t\bar{t}h$ production only, while the remaining operators affect all considered processes. While the constraining power of Higgs data for these operators, which appear at NLO only, is generally small, we find that in particular the bounds on $C_{qu}^{(1)}$ tighten with the inclusion of these NLO effects.

Moreover, we include NLO contributions from C_H to total Higgs production and decay channels [85, 86]. However, this only marginally affects the results as the constraints on C_H are dominated by di-Higgs production.

5.2 Global fit

In Figure 3, we present a comparison of the global fit at LO with the one including partial NLO SMEFT predictions. The corresponding numerical fit results can be found in Table 7 in appendix D. The bounds on most operators are only mildly influenced by the inclusion of NLO SMEFT predictions. However, in the four-quark sector the limits on the Wilson coefficients $C_{qd}^{(1)}, C_{qu}^{(1)}, C_{ud}^{(1)}$ and, to a smaller extent, C_{uu} significantly tighten when improving the SMEFT predictions to NLO precision and are now below $|C|/\Lambda^2 < 10/\text{TeV}^2$.

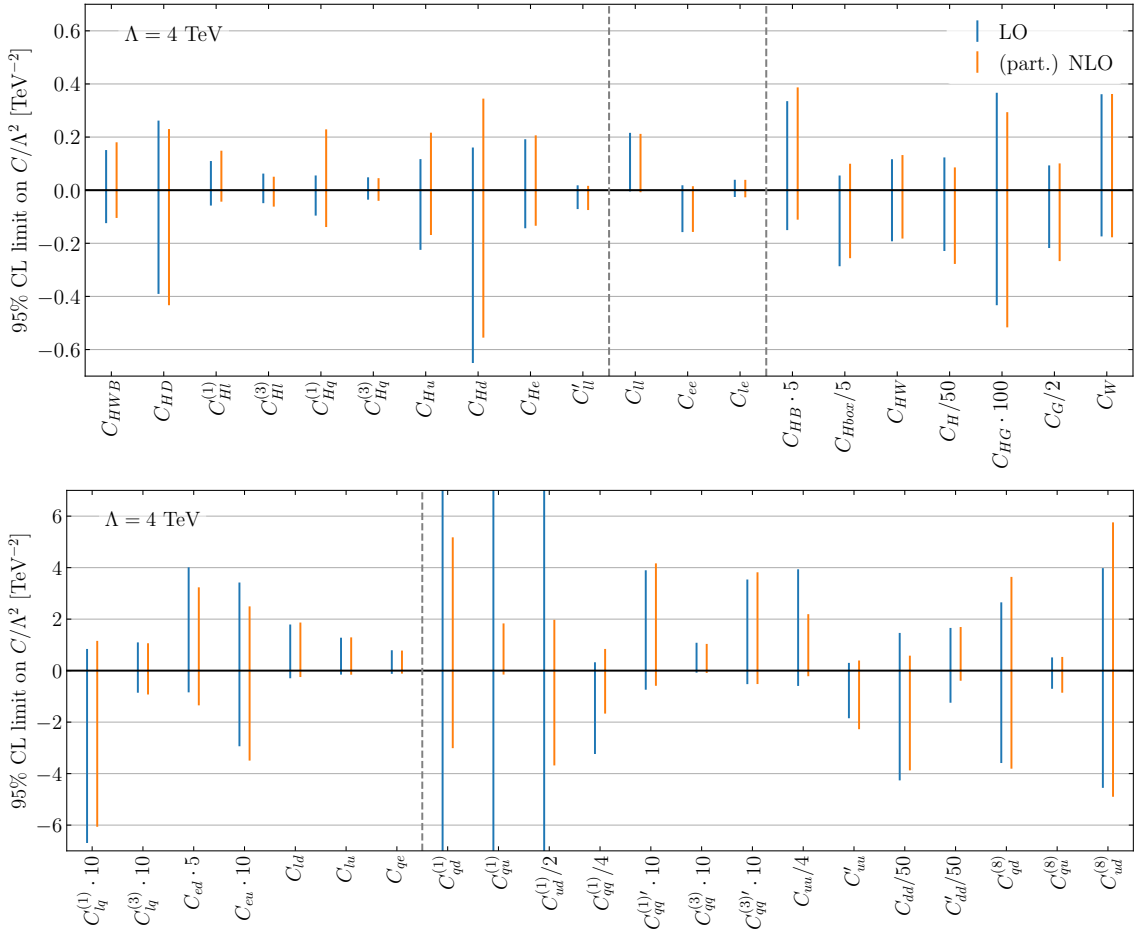


Figure 3: Comparison of the global analysis at LO with the one including partial NLO predictions.

The Wilson coefficients C_{dd} and C'_{dd} remain the only ones exceeding this limit. On the other hand, the bounds on $C_{Hq}^{(1)}$ are weakened by a factor 2.5 through its correlations with four-quark operators in EWPO, in particular with $C_{qq}^{(1)}$ and C_{uu} . We show these correlations arising at NLO in Figure 4. At LO, there are no visible correlations between $C_{Hq}^{(1)}$ and the four-quark operators as indicated by the blue contours. At NLO, shown in orange, a strong correlation with $C_{qq}^{(1)}$ and an anti-correlation with C_{uu} are induced through the EWPO SMEFT predictions, weakening the limits on $C_{Hq}^{(1)}$.

All 41 Wilson coefficients remain consistent with the SM within 2σ in the NLO fit. However, the number of Wilson coefficients exhibiting deviations exceeding 1.5σ grows from six to nine

$$\{C_{ll}, C_{ee}, C_{lu}, C_{qq}^{(3)}, C_{ld}, C_{qu}^{(1)}, C_{qq}^{(1')}, C_{qq}^{(3')}, C_{uu}\}, \quad (5.4)$$

where we have greyed out the Wilson coefficients which already deviated from zero in the LO fit, see Equation (4.2). Two coefficients, which exhibit deviations $\geq 1.5\sigma$ in the LO fit are shifted towards more SM-like values at NLO, $C_{qq}^{(1)}$ and $C_{lq}^{(1)}$. For $C_{qq}^{(1)}$, this is due to its

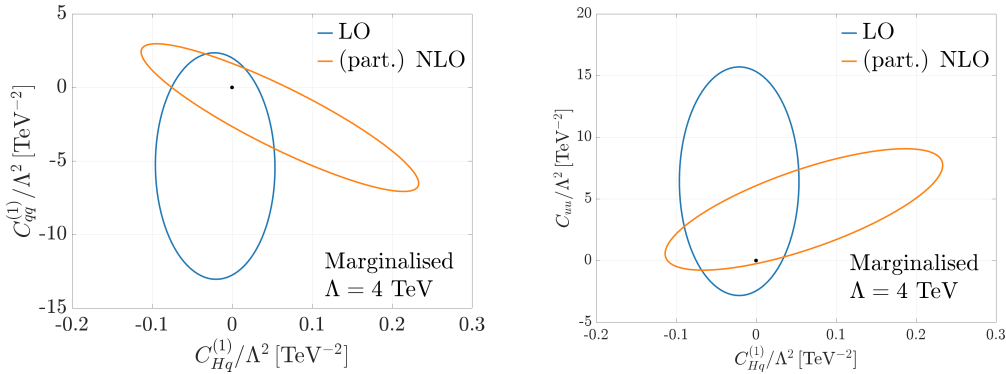


Figure 4: 95% CI limits in the LO and partial NLO analyses showing the correlations of $C_{Hq}^{(1)}$ with $C_{qq}^{(1)}$ (left) and C_{uu} (right).

additional NLO contributions to EWPO, Higgs and top data. The shift of $C_{lq}^{(1)}$ towards more SM-like values in the NLO fit is the result of EWPO data. On the other hand, $C_{qu}^{(1)}$, which at NLO is strongly constrained by Higgs data, deviates due to experimental deviations in $t\bar{t}H$ production. C_{uu} experiences a shift away from zero in both the LO and NLO analyses, which is caused by the dijet dataset. However, the shift becomes more apparent at NLO, where the overall bounds on this parameter shrink as a result of stronger limits on other correlated four-quark operators. For $C_{qq}^{(1)prime}$, which is dominantly affected by $t\bar{t}V$, and $C_{qq}^{(3)prime}$, which is mainly shifted by both $t\bar{t}V$ and dijet data, the change of the limits between the LO and NLO analysis is only marginal, the central values are shifted by 13% and 9%, respectively. The same is true for the semileptonic operator C_{ld} , for which the central value only changes by 8%.

We have again checked explicitly that when conducting a fit without the five most poorly constrained operators, $C_{qd}^{(1)}$, $C_{ud}^{(1)}$, $C_{qu}^{(1)}$, C_{dd} and C_{dd}^{prime} , limits on the remaining operators exhibit no significant changes. The only noticeable effects are on four-quark operators for which the corresponding limits strengthen by up to 33% when removing the five least constrained operators from the fit. Moreover, the limit on C_G changes by 17% and the limit on $C_{Hq}^{(1)}$, which suffers from large correlations in the global analysis, receives a 35% correction. This highlights the robustness of the results even though some operators remain weakly limited given the current dataset.

In Figure 5 we present the ratio of the uncertainties on the Wilson coefficients in a global fit over the uncertainties in a one-parameter fit. This can be seen as a measure of the sensitivity of each operator on correlations with the remaining ones. As expected, we find that the bounds on many operators are significantly weakened in the global analysis. Limits on semileptonic operators and four-quark operators involving right-handed quark fields only, typically increase by more than a factor 20 in a global fit. For semileptonic operators, this is due to the Drell-Yan dataset imposing tight constraints at the one-parameter level, while only poorly disentangling the effects of different operators. We will further discuss this in Section 6.2. Of those operators affecting EWPO at LO, C_{HWB} and C_{HD} have the largest degeneracies and the corresponding limits increase by factors 44 and

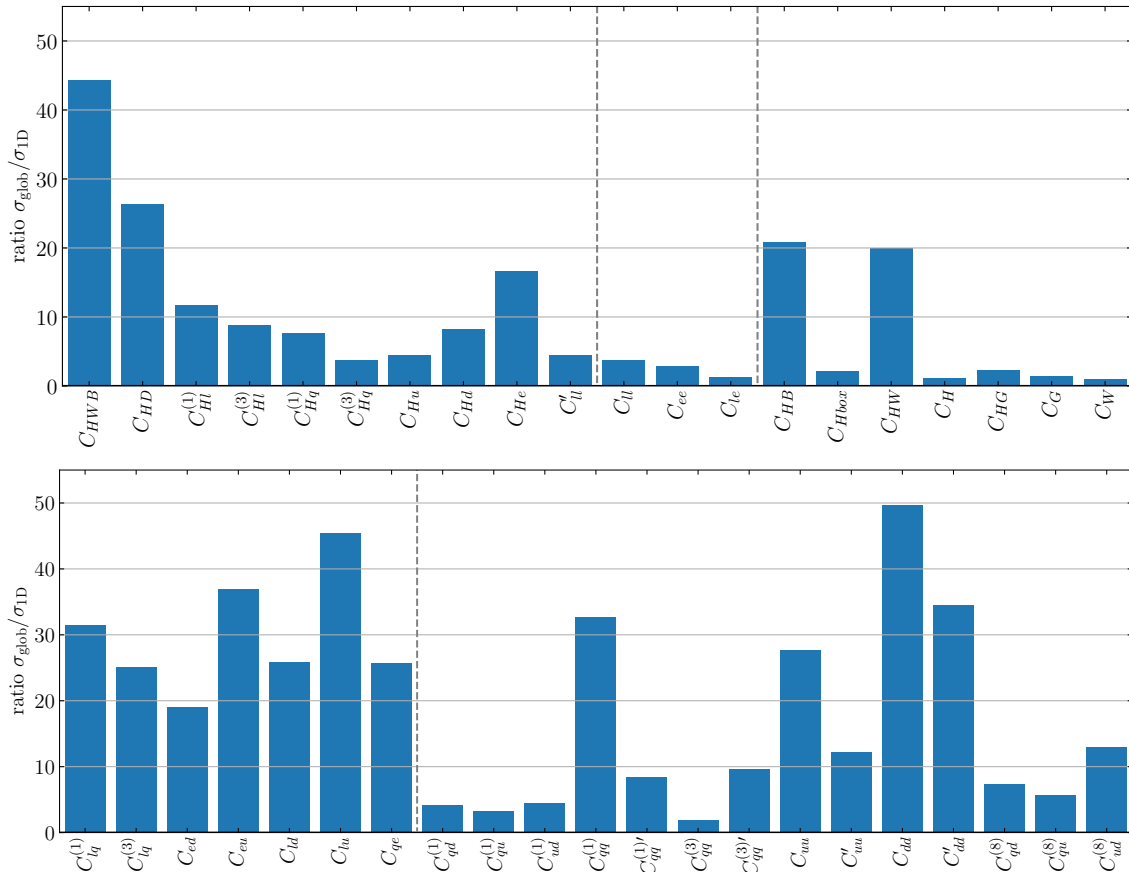


Figure 5: Ratio of the uncertainties on the Wilson coefficients in a global 41-parameter analysis over the uncertainties in a single-parameter analysis (both including partial NLO predictions). This can be interpreted as a measure of the relevance of correlations with the remaining Wilson coefficients in the analysis.

26, respectively, in a global fit. In the Higgs-gauge sector, only C_{HW} and C_{HB} , which have large correlations with C_{HWB} and C_{HD} , see also the correlation matrix in Figure 14, are significantly weakened in the global analysis by factors of 20 and 21, respectively. The operators whose limits are most stable under a global analysis are C_{le} , C_H , C_G and C_W . The corresponding limits change by less than 50 % in a global fit.

6 Interplay between the datasets

The datasets described in Section 3 are sensitive to different, and often unique, directions in parameter space. The combination of different datasets hence plays a crucial role for the limits obtained in a global analysis. In this Section, we will discuss the constraining power of the individual datasets as well as their interplay.

In Figure 6, we once again display the results of the comprehensive global analysis encompassing all 41 Wilson coefficients. In addition to the global analysis including all datasets, we use different colours to represent fits with the exclusion of a single dataset to

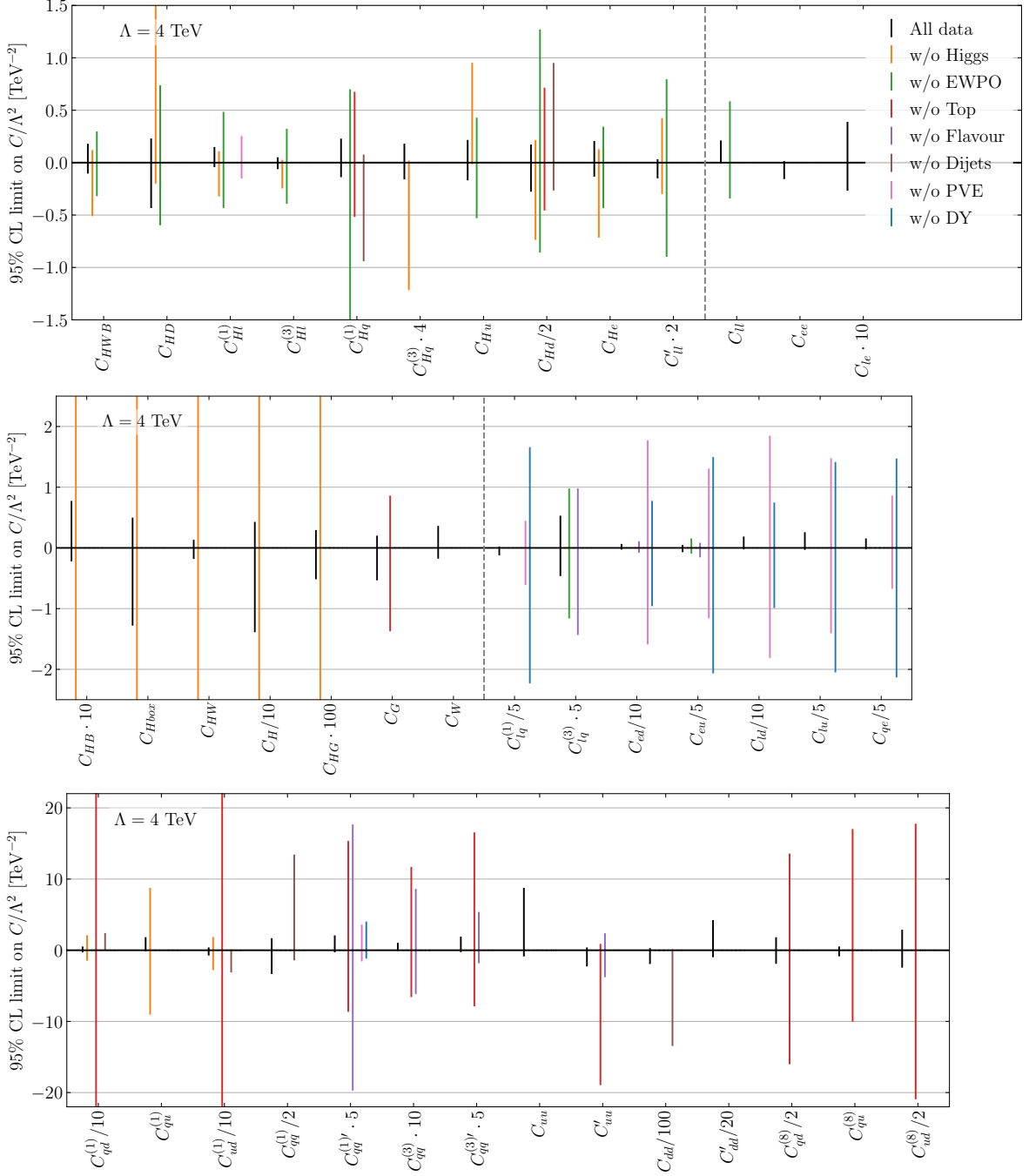


Figure 6: Global analysis including NLO predictions. Different colours correspond to analyses removing certain datasets to highlight their relevance. Note that some Wilson coefficients have been rescaled and that the y-axis range is different in the three plot panels.

highlight the relevance of the respective set. To ensure a better readability of the plot, we exclusively display bounds in cases where the removal of a dataset impacts the constrained

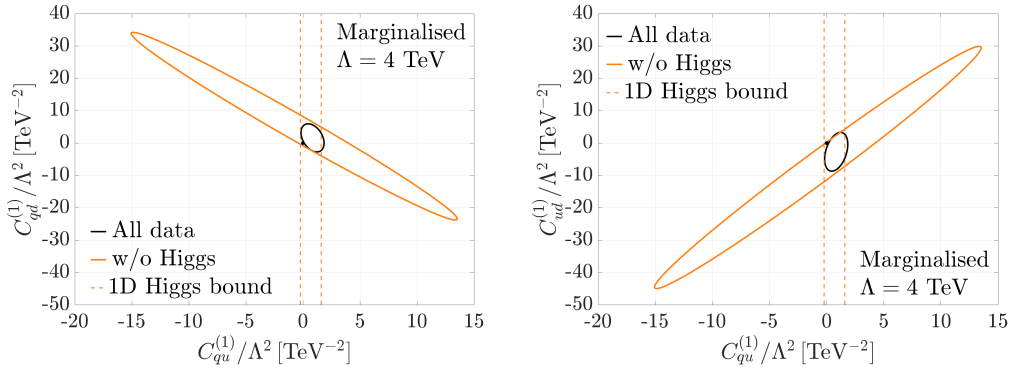


Figure 7: 95% CI limits with and without the inclusion of the Higgs dataset showing the impact of this dataset on $C_{qd}^{(1)}$ (left) and $C_{ud}^{(1)}$ (right) through lifting correlations with $C_{qu}^{(1)}$.

range by a minimum of 100 %. As expected, the ten operators contributing to EWPO at LO, displayed in the upper panel, are dominantly constrained by EWPO and Higgs physics, corresponding to the orange and green lines, respectively. However, we see that the other datasets, such as PVE (pink), top (red) and dijets (brown), are also crucial for constraining some of these operators. For $C_{HI}^{(1)}$, the relevance of the PVE dataset is a result of correlations with semileptonic operators and will be further explored in Section 6.1. For C_{Hd} and $C_{Hq}^{(1)}$, correlations in EWPO with four-quark operators ($C_{Hq}^{(1)}$ with $C_{qq}^{(1)}$, C_{uu} and C_{Hd} with the weakly constrained C_{dd}) lead to relevant contributions from top and dijet observables.

Four-lepton operators are dominantly constrained in lepton-scattering experiments and EWPO. By constraining C_{ll}^i , EWPO also play an important role in disentangling the correlations with C_{ll} present in lepton scattering.

Operators contributing to modified Higgs couplings, shown in the central panel, do not receive important contributions from any other sector. C_G and C_W are dominantly constrained in top physics and Zjj production (the latter is not shown as an individual dataset), respectively.

Semileptonic operators, also displayed in the central panel, are all dominantly constrained by PVE and Drell-Yan, except $C_{lq}^{(3)}$ and C_{eu} which receive important contributions from the flavour sector as well as EWPO. We study the interplay of PVE and Drell-Yan further in Section 6.2.

Interestingly, four-quark operators, displayed in the lower panel, receive important constraints from all considered datasets except EWPO. For most operators the most dominant constraints result from Higgs, top, dijet and flavour data. Higgs physics plays an important role in setting the limits on $C_{qd}^{(1)}$, $C_{qu}^{(1)}$, $C_{ud}^{(1)}$, even though only $C_{qu}^{(1)}$ is directly constrained in Higgs physics (through NLO $t\bar{t}h$ production). The effect on the other two operators is the result of strong correlations with $C_{qu}^{(1)}$ as shown in Figure 7. The orange contours correspond to a global analysis without Higgs data and show a strong correlation between the considered four-quark operators. Limits on $C_{qu}^{(1)}$ from Higgs physics, indicated by the dashed lines, break this degeneracy. The combination of all datasets (black con-

tours) therefore not only enhances the limits on $C_{qu}^{(1)}$ but also influences the correlated coefficients $C_{qd}^{(1)}$ and $C_{ud}^{(1)}$.

For $C_{qd}^{(1)}$, $C_{ud}^{(1)}$, $C_{qq}^{(1)}$, C_{dd} , dijet data have a relevant impact for breaking degeneracies between operators and shifting the limits towards SM values. Without dijet data, deviations in $t\bar{t}h$ production push the limits towards non-SM values. For C_{dd}' , which can only be very weakly constrained, the changes of the limits when removing the EWPO and dijet dataset are smaller than the chosen threshold of two (100%). Therefore, no dataset-specific additional limits are shown in the plot. Somewhat surprisingly, Drell-Yan and PVE influence the bounds on $C_{qq}^{(1)'$. We further investigate this effect in Section 6.2.

6.1 EWPO and PVE datasets

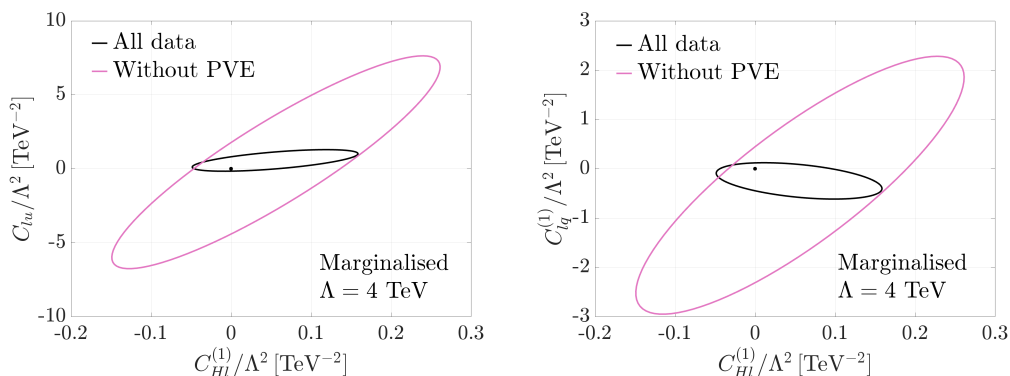


Figure 8: 95% CI limits with and without the inclusion of the PVE dataset showing the impact of this dataset on $C_{Hl}^{(1)}$ through lifting correlations with C_{lu} and $C_{lq}^{(1)}$.

At LO, the operators contributing to the description of EWPO are tightly constrained. At NLO, the number of operators contributing to EWPO extends from ten to 35, hence adding a lot more freedom to the fit. The additional degrees of freedom need to be constrained by other datasets, otherwise the limits on the operators appearing at LO will be degraded. PVE plays an important role in constraining semileptonic operators and lifting degeneracies between these and the operators entering EWPO at LO. We illustrate two examples of the breaking of this degeneracy in Figure 8. The pink contours show large correlations between $C_{Hl}^{(1)}$ and C_{lu} (left panel) as well as $C_{lq}^{(1)}$ (right panel) when PVE data are absent from the fit. By setting strong constraints on C_{lu} and $C_{lq}^{(1)}$ and testing different directions in the $C_{Hl}^{(1)}-C_{lu}/C_{lq}^{(1)}$ parameter space, PVE has an important impact on the global analyses bounds of $C_{Hl}^{(1)}$, see Figure 6.

In [87–89], it was shown that the inclusion of β -decay observables and semileptonic meson decays [90, 91] can have an interesting interplay with EWPO. In appendix A, we estimate this effect by adding Δ_{CKM} as a pseudo-observable to our fit.

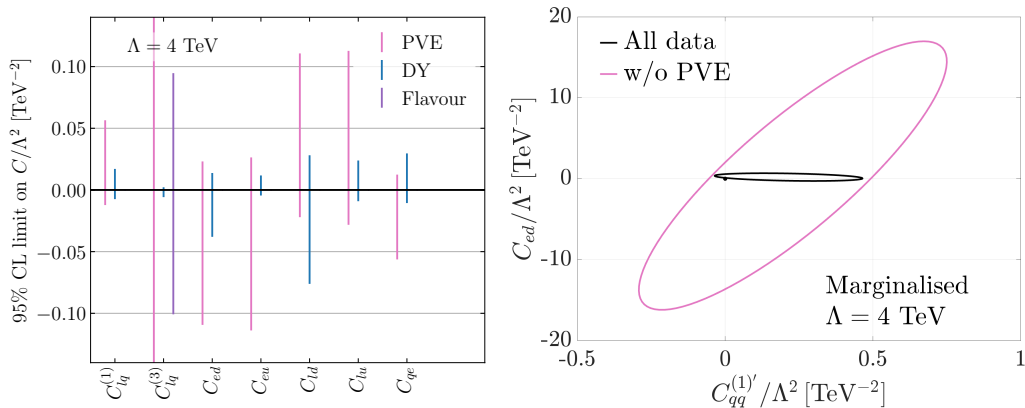


Figure 9: (Incomplete) list of single-parameter bounds at 95% CL on semileptonic operators (left). Note that for the flavour dataset we suppress the limits on all operators except $C_{lq}^{(3)}$ because they are not competitive with PVE and Drell-Yan. 95% CI limits with and without the inclusion of the PVE dataset showing the impact of this dataset on $C_{qq}^{(1)'}$ through lifting correlations with C_{ed} (right).

6.2 Drell-Yan, PVE and flavour datasets

Drell-Yan and PVE data are both sensitive to semileptonic operators

$$\{C_{lq}^{(1)}, C_{lq}^{(3)}, C_{ed}, C_{eu}, C_{ld}, C_{lu}, C_{qe}\}. \quad (6.1)$$

We present single-parameter fit results for both datasets in Figure 9. For $C_{lq}^{(3)}$, we also show limits from the flavour dataset, which are competitive for this coefficient. Constraints from Drell-Yan dominate over those from PVE throughout the whole parameter space. Nevertheless, limits from PVE are of a similar order of magnitude and this dataset plays an important role in the global analysis through its ability to test different directions in parameter space compared to Drell-Yan. To highlight the complementarity of both searches, we present 2D-limit plots for C_{lu} -vs- C_{qe} and $C_{lq}^{(3)}$ -vs- C_{eu} in Figure 10. In a two-parameter fit, shown by the filled contours, we find that PVE (pink) and Drell-Yan (blue) probe almost orthogonal directions in parameter space for C_{qe} and C_{lu} . In Drell-Yan, these two Wilson coefficients appear with the same sign as they are both dominated by up-type quark contributions, which leads to an anti-correlation of C_{qe} and C_{lu} . Only exclusive down-type quark contributions, C_{ed} and C_{ld} , as well as the structurally distinct $C_{lq}^{(3)}$ enter with an opposite sign for Drell-Yan. The PVE dataset is sensitive to axial couplings in the quark or lepton sector. As the operators corresponding to C_{qe} and C_{lu} involve quarks and leptons of different chiralities, all PVE observables will be sensitive to a negative relative combination of these two operators (whenever both operators appear), which results in a positive correlation of the Wilson coefficients. The complementarity between the PVE and Drell-Yan datasets also remains when marginalising over additional semileptonic Wilson coefficients. This is shown by the unfilled contours in the left panel of Figure 10. Comparing Figure 6, we find that PVE is particularly relevant for the semileptonic operators specifically

involving down-type quarks since the corresponding measurements do not experience the same parton distribution function (PDF) suppression as Drell-Yan.

In the right panel of Figure 10, we show the two-parameter limits on $C_{lq}^{(3)}$ -vs- C_{eu} when marginalising over $C_{lq}^{(1)}$, C_{lu} and C_{qe} . Again, Drell-Yan and PVE probe complementary directions in parameter space. In addition, flavour plays an important role by setting constraints on $C_{lq}^{(3)}$.

Even when combining all datasets, the limits on almost all semileptonic operators are weakened by a more than a factor 20 in the global analysis, see Figure 5. The Drell-Yan dataset delivers strong individual constraints on semileptonic operators. However, different bins and final states of the distributions only have a marginal impact on the relative importance of different Wilson coefficients of semileptonic operators. Therefore, this dataset is particularly affected by correlations. Therefore, in order to further improve bounds on semileptonic operators, it is relevant to add observables constraining different combinations of the corresponding Wilson coefficients.

The complementarity between low-energy Parity-Violating Electron Scattering (PVES) and LHC Run I Drell-Yan data in constraining semileptonic operators has already been studied in [92]. While this previous work is based on LHC Run I data up to 1.5 TeV, our analysis includes LHC Run II data up to an invariant-mass of 3 TeV.

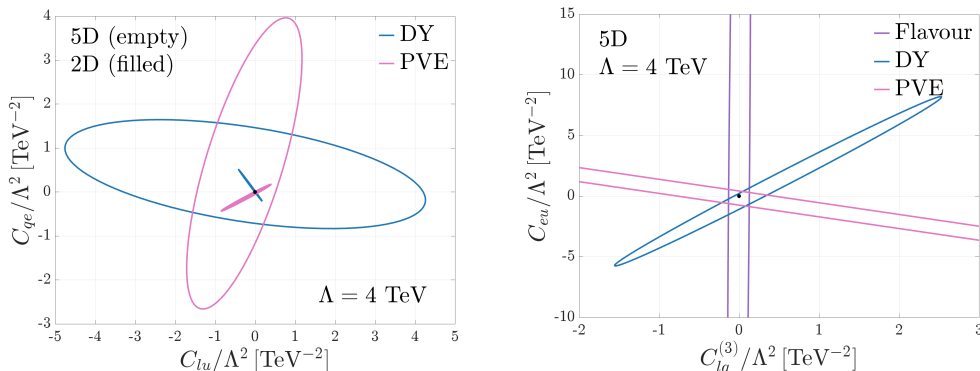


Figure 10: 95% CI contours on the two-dimensional parameter space of the semileptonic operators from PVE and Drell-Yan (and flavour). The 5D analyses are marginalised over the Wilson coefficients $C_{lq}^{(1)}$, $C_{lq}^{(3)}$ and C_{eu} (left) and $C_{lq}^{(1)}$, C_{lu} and C_{qe} (right).

In addition to setting limits on semileptonic operators, we have observed in Figure 6 that the PVE and Drell-Yan datasets also affect bounds on the four-quark operator $C_{qq}^{(1)'}$ even though they are not directly sensitive to this coefficient. To explain this feature, we report in the right panel of Figure 9 the 2D-limits on $C_{qq}^{(1)'}$ -vs- C_{ed} . In a global fit without PVE data, these two operators are correlated as shown by the pink contour. PVE sets a stringent constraint on C_{ed} which in turn improves the bounds on $C_{qq}^{(1)'}$ significantly, see the black contour.

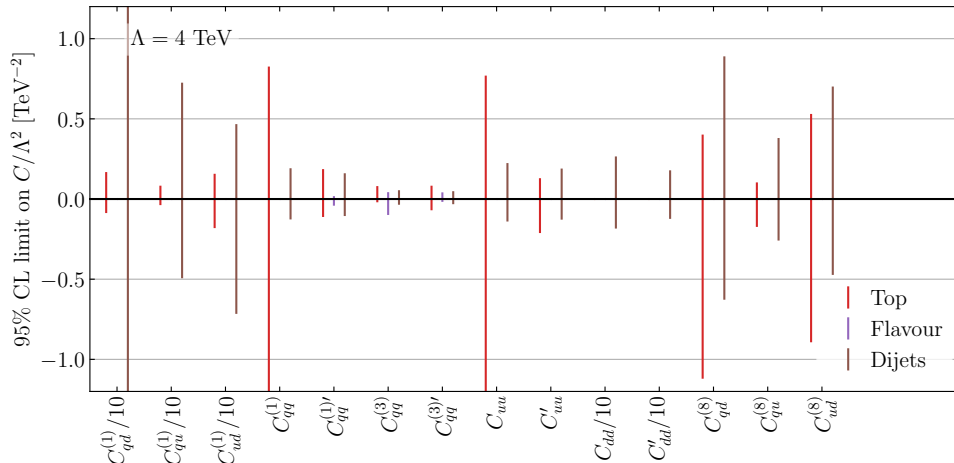


Figure 11: Single-operator bounds at 95% CL on the Wilson coefficients of the four-quark operators from different datasets.

6.3 Top, flavour and dijet datasets

Top, flavour and dijet data overlap in their sensitivity to four-quark operators. In the following, we will discuss in how far the bounds from these sectors are complementary in a global fit, focusing in particular on the interplay of top and flavour data.

We compare the one-parameter bounds on the relevant Wilson coefficients in Figure 11. At the single-parameter level, top (red) and dijet (brown) data are equally relevant for constraining four-quark operators. However, at the level of a global fit, limits from top physics typically dominate and dijet data is mainly relevant to set limits on operators which do not contribute to top physics such as those involving only down-type quarks, see Figure 6. The flavour dataset (purple) has a crucial impact on the bounds on $C_{qq}^{(1)'}$ and $C_{qq}^{(3)'}$ even in our $U(3)^5$ symmetric scenario, setting the strongest one-parameter bounds on these operators and having a strong effect in the global analysis as well. For these two parameters, flavour data can only constrain the direction $C_{qq}^{(1)'} - C_{qq}^{(3)'}$, which contributes at tree-level to C_1 and at one-loop to C_9 and C_{10} , see appendix E for the definitions of these LEFT coefficients. This can be explained by the fact that only structures with one up-type and one down-type quark bilinear $(\bar{u}\gamma_\mu u)_L(\bar{d}\gamma^\mu d)_L$ with colour indices contracted within the brackets contribute to flavour observables, for which $C_{qq}^{(1)'}$ and $C_{qq}^{(3)'}$ have exactly opposite signs. On the other hand, $t\bar{t}$ production receives contributions from both the above structure and from its equivalent with two up-type quark bilinears. The latter, to which $C_{qq}^{(1)'}$ and $C_{qq}^{(3)'}$ both contribute with the same sign, dominates due to the larger up-type PDFs. As a result, $C_{qq}^{(1)'}$ and $C_{qq}^{(3)'}$ have a positive relative sign in all considered $t\bar{t}$ observables. We show the complementary behaviour of top and flavour data in Figure 12. The filled contours correspond to fitting $C_{qq}^{(1)'}$ and $C_{qq}^{(3)'}$ only, whereas the empty contours have been obtained in a 14-parameter fit marginalising over the remaining twelve four-quark operators. We can see that while the limits are degraded in a global fit, as expected, the complementarity of the flavour and top datasets persists. Therefore, both datasets are

essential in order to perform a global analysis including these two operators. See also [30] on resolving the flavour structure of the four-quark operators $Q_{qq}^{(1)}$ and $Q_{qq}^{(3)}$ including higher-order terms of the MFV expansion using similar datasets⁵.

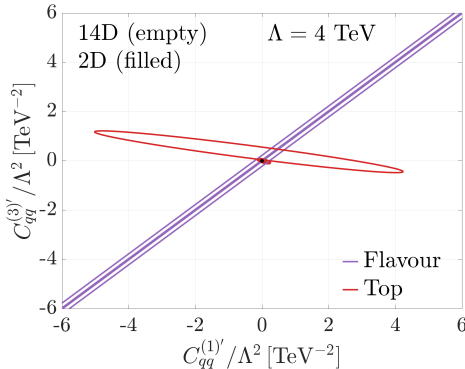


Figure 12: 95% CI contours of $C_{qq}^{(1)'}$ vs $C_{qq}^{(3)'}$ from flavour and top data. See text for details.

In our work, the flavour dataset mostly affects bounds on the operators of the four-quark sector. When going beyond our minimal MFV hypothesis, flavour data has been shown to play an important role for constraining higher-order terms in the MFV expansion of semileptonic and gauge-fermion operators [29, 31, 33].

7 Conclusions and outlook

We conducted a global analysis of all 41 operators of the minimal MFV SMEFT, i.e. assuming an exact $U(3)^5$ symmetry at the high scale. The selection of our Wilson-coefficient set is entirely guided by theory and no flat directions remain in the fit when considering EWPO, Higgs, top, flavour, dijet, PVE, Drell-Yan and lepton scattering datasets. In an analysis based solely on LO SMEFT predictions, five four-quark operators involving right-handed fermion fields remain weakly constrained in our global fit. However, their presence in the fit does not significantly impact the limits on the remaining operators, highlighting that there is only minimal crosstalk between both Wilson-coefficient sets.

Including partial NLO SMEFT predictions enables us to test the four-quark operators which only contribute weakly to our observables at LO. With partial NLO SMEFT corrections, only the Wilson coefficients C_{dd} and C'_{dd} exhibit bounds on C/Λ^2 weaker than $10/\text{TeV}^2$. These two Wilson coefficients are highly anti-correlated. For another ten operators, the bounds are weaker than $1/\text{TeV}^2$, the remaining 29 operators can be constrained to $|C|/\Lambda^2 < 1/\text{TeV}^2$. All 41 Wilson coefficients remain consistent with the SM within 2σ in the LO and NLO analyses. Six (nine) Wilson coefficients exhibit deviations exceeding 1.5σ in the LO (NLO) fit.

In principle, switching to NLO SMEFT predictions introduces additional degeneracies between operators as a single observable is a function of a larger set of Wilson coefficients at

⁵Our parameters $C_{qq}^{(x)'}$ correspond to $(\widetilde{aa})^{(x)}$ in their notation.

NLO. For the EWPO dataset, the number of relevant flavour-symmetric Wilson coefficients increases from ten at LO to 35 at NLO. Nevertheless, for most Wilson-coefficient bounds the impact of going to NLO precision in the EWPO dataset is weak. This shows that constraints on the operators first appearing at NLO in EWPO from other sectors are strong enough to render the effect of the additional degeneracies subdominant. Of the operators constrained at LO in EWPO, only the limit on $C_{Hq}^{(1)}$ is impacted significantly by correlations with four-quark operators induced at NLO and increases by a factor 2.5.

The limits on semileptonic operators strongly increase in the global fit compared to single-parameter fits. This is due to Drell-Yan providing very strong single-parameter limits, while only very poorly disentangling the effects of different semileptonic operators, as these typically experience the same dependence on the considered energy and final-state flavour. The combination of Drell-Yan with PVE data, which provides weaker limits at a single-parameter fit level, is highly relevant to constrain semileptonic operators in a global analysis, as it allows to break the degeneracies present in the Drell-Yan dataset. In the bosonic sector, the largest limit increases in a global fit compared to a single-parameter fit occur for C_{HWB} , C_{HD} , C_{HB} and C_{HW} .

Limits on four-quark operators, particularly those involving down-type quarks, profit from the inclusion of dijet data. To avoid large quadratic Wilson-coefficient contributions and therefore a potential violation of the EFT validity, we recast an ATLAS dijet+photon search [74], which probes the low- m_{jj} invariant-mass range. SMEFT predictions for this differential distribution are included as an ancillary file with the arXiv submission. Data from flavour as well as top physics test complementary directions in the four-quark operator space. Therefore, their combination is essential to fully constrain the NP parameter space.

In the future, it would be interesting to consider all SMEFT observables at NLO precision and include renormalisation group running effects beyond the flavour sector [93].

Our results show the necessity of combining numerous datasets at different scales for global SMEFT analyses. Datasets which seem subdominant at the single-parameter fit level can play a significant role in disentangling directions in the Wilson coefficient parameter space.

Acknowledgements

We thank Luca Mantani and Ken Mimasu for their invaluable assistance in comparing the SMEFit and fitmaker theory predictions and the authors of [82] for providing additional NLO SMEFT predictions. All three authors are supported by the Cluster of Excellence “Precision Physics, Fundamental Interactions, and Structure of Matter” (PRISMA⁺ EXC 2118/1) funded by the German Research Foundation (DFG) within the German Excellence Strategy (Project ID 390831469). A.B. also gratefully acknowledges support from the Alexander-von-Humboldt foundation as a Feodor Lynen Fellow during large parts of this project. T.H. also thanks the CERN theory group for its hospitality during his regular visits to CERN where part of the work was done.

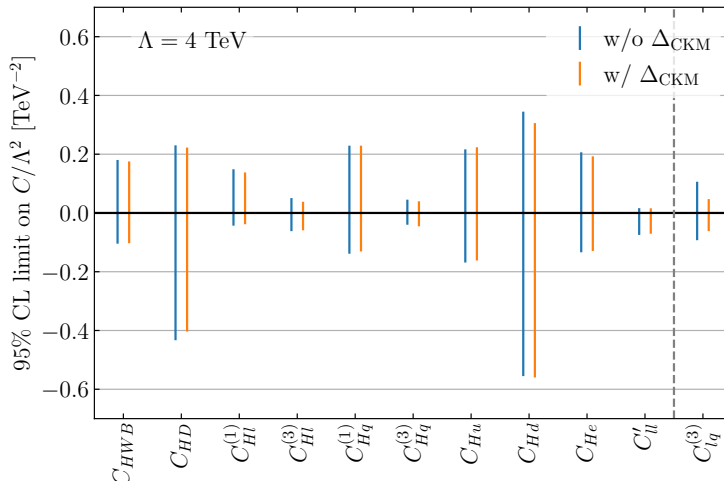


Figure 13: Global analysis of all 41 Wilson coefficients with and without the inclusion of Δ_{CKM} as an observable. Only the ten Wilson coefficients contributing to EWPO at LO and $C_{lq}^{(3)}$ are shown.

A Δ_{CKM} as an additional low-energy observable

Observables from β -decay and semileptonic meson decays [90, 91] have been shown to have interesting interplay with EWPO [87–89]. In this section, we estimate the effect of including these measurements by adding a single pseudo-observable to our fit. The unitarity of the CKM matrix experiences a 2σ deviation from zero [94]

$$\Delta_{\text{CKM}} = |V_{ud}|^2 + |V_{us}|^2 - 1 = -0.0015 \pm 0.0007, \quad (\text{A.1})$$

where V_{ud} is dominantly constrained by superallowed nuclear β decays and V_{us} receives the strongest constraints from semileptonic Kaon decays. In the SMEFT, the measurements of V_{ij} are influenced by modifications of the W -boson couplings as well as four-fermion operator contributions

$$\Delta_{\text{CKM}} = 2 \frac{v^2}{\Lambda^2} \left(C_{Hq}^{(3)} - C_{Hl}^{(3)} + C'_{ll} - C_{lq}^{(3)} \right). \quad (\text{A.2})$$

Including Δ_{CKM} as a pseudo-observable and performing a fit, we find only a mild influence on most operators in our 41-parameter fit. The corresponding limits are shown in Figure 13. Only the limits on $C_{lq}^{(3)}$ and $C_{Hl}^{(3)}$ are influenced by more than 10% and decrease by factors of 0.55 and 0.86, respectively. Decreasing the parameter set to the eleven coefficients explicitly shown in Figure 13 and removing the Higgs dataset, we find a stronger impact of the observable Δ_{CKM} with four of the coefficients contributing to EWPO at LO changing by more than 10%, thus confirming the findings of [87, 89]. $C_{lq}^{(3)}$ is tightly constrained by Drell-Yan data in the eleven-parameter fit and therefore changes by less than 5% when including Δ_{CKM} as a pseudo-observable in this case.

It would be interesting to properly include observables from β -decay and semileptonic meson decays [90, 91] in the global analysis, even though we expect the impact to be diminished with respect to low-dimensional Wilson-coefficient analyses [87, 89].

B Flavour symmetric and CP even operators

1 : X^3		2 : H^6		3 : $H^4 D^2$	
Q_G	$f^{ABC} G_\mu^{A\nu} G_\nu^{B\rho} G_\rho^{C\mu}$	Q_H	$(H^\dagger H)^3$	$Q_{H\Box}$	$(H^\dagger H)\Box(H^\dagger H)$
Q_W	$\epsilon^{IJK} W_\mu^{I\nu} W_\nu^{J\rho} W_\rho^{K\mu}$			Q_{HD}	$(H^\dagger D_\mu H)^* (H^\dagger D_\mu H)$
4 : $X^2 H^2$		7 : $\psi^2 H^2 D$			
Q_{HG}	$H^\dagger H G_{\mu\nu}^A G^{A\mu\nu}$	$Q_{Hl}^{(1)}$	$(H^\dagger i \overleftrightarrow{D}_\mu H)(\bar{l}_p \gamma^\mu l_p)$		
Q_{HW}	$H^\dagger H W_{\mu\nu}^I W^{I\mu\nu}$	$Q_{Hl}^{(3)}$	$(H^\dagger i \overleftrightarrow{D}_\mu^I H)(\bar{l}_p \tau^I \gamma^\mu l_p)$		
Q_{HB}	$H^\dagger H B_{\mu\nu} B^{\mu\nu}$	Q_{He}	$(H^\dagger i \overleftrightarrow{D}_\mu H)(\bar{e}_p \gamma^\mu e_p)$		
Q_{HWB}	$H^\dagger \tau^I H W_{\mu\nu}^I B^{\mu\nu}$	$Q_{Hq}^{(1)}$	$(H^\dagger i \overleftrightarrow{D}_\mu H)(\bar{q}_p \gamma^\mu q_p)$		
		$Q_{Hq}^{(3)}$	$(H^\dagger i \overleftrightarrow{D}_\mu^I H)(\bar{q}_p \tau^I \gamma^\mu q_p)$		
		Q_{Hu}	$(H^\dagger i \overleftrightarrow{D}_\mu H)(\bar{u}_p \gamma^\mu u_p)$		
		Q_{Hd}	$(H^\dagger i \overleftrightarrow{D}_\mu H)(\bar{d}_p \gamma^\mu d_p)$		
8 : $(\bar{L}L)(\bar{L}L)$		8 : $(\bar{R}R)(\bar{R}R)$		8 : $(\bar{L}L)(\bar{R}R)$	
$Q_{\ell\ell}$	$(\bar{l}_p \gamma_\mu l_p)(\bar{l}_s \gamma^\mu l_s)$	Q_{ee}	$(\bar{e}_p \gamma_\mu e_p)(\bar{e}_s \gamma^\mu e_s)$	Q_{le}	$(\bar{l}_p \gamma_\mu l_p)(\bar{e}_s \gamma^\mu e_s)$
$Q'_{\ell\ell}$	$(\bar{l}_p \gamma_\mu l_s)(\bar{l}_s \gamma^\mu l_p)$	Q_{uu}	$(\bar{u}_p \gamma_\mu u_p)(\bar{u}_s \gamma^\mu u_s)$	Q_{lu}	$(\bar{l}_p \gamma_\mu l_p)(\bar{u}_s \gamma^\mu u_s)$
$Q_{qq}^{(1)}$	$(\bar{q}_p \gamma_\mu q_p)(\bar{q}_s \gamma^\mu q_s)$	Q'_{uu}	$(\bar{u}_p \gamma_\mu u_s)(\bar{u}_s \gamma^\mu u_p)$	Q_{ld}	$(\bar{l}_p \gamma_\mu l_p)(\bar{d}_s \gamma^\mu d_s)$
$Q_{qq}^{(3)}$	$(\bar{q}_p \gamma_\mu \tau^I q_p)(\bar{q}_s \gamma^\mu \tau^I q_s)$	Q_{dd}	$(\bar{d}_p \gamma_\mu d_p)(\bar{d}_s \gamma^\mu d_s)$	Q_{qe}	$(\bar{q}_p \gamma_\mu q_p)(\bar{e}_s \gamma^\mu e_s)$
$Q_{qq}^{(1)'}$	$(\bar{q}_p \gamma_\mu q_p)(\bar{q}_s \gamma^\mu q_s)$	Q'_{dd}	$(\bar{d}_p \gamma_\mu d_s)(\bar{d}_s \gamma^\mu d_p)$	$Q_{qu}^{(1)}$	$(\bar{q}_p \gamma_\mu q_p)(\bar{u}_s \gamma^\mu u_s)$
$Q_{qq}^{(3)'}$	$(\bar{q}_p \gamma_\mu \tau^I q_s)(\bar{q}_s \gamma^\mu \tau^I q_p)$	Q_{eu}	$(\bar{e}_p \gamma_\mu e_p)(\bar{u}_s \gamma^\mu u_s)$	$Q_{qu}^{(8)}$	$(\bar{q}_p \gamma_\mu T^A q_p)(\bar{u}_s \gamma^\mu T^A u_s)$
$Q_{lq}^{(1)}$	$(\bar{l}_p \gamma_\mu l_p)(\bar{q}_s \gamma^\mu q_s)$	Q_{ed}	$(\bar{e}_p \gamma_\mu e_p)(\bar{d}_s \gamma^\mu d_s)$	$Q_{qd}^{(1)}$	$(\bar{q}_p \gamma_\mu q_p)(\bar{d}_s \gamma^\mu d_s)$
$Q_{lq}^{(3)}$	$(\bar{l}_p \gamma_\mu \tau^I l_p)(\bar{q}_s \gamma^\mu \tau^I q_s)$	$Q_{ud}^{(1)}$	$(\bar{u}_p \gamma_\mu u_p)(\bar{d}_s \gamma^\mu d_s)$	$Q_{qd}^{(8)}$	$(\bar{q}_p \gamma_\mu T^A q_p)(\bar{d}_s \gamma^\mu T^A d_s)$
		$Q_{ud}^{(8)}$	$(\bar{u}_p \gamma_\mu T^A u_p)(\bar{d}_s \gamma^\mu T^A d_s)$		

Table 2: Flavour symmetric and CP even dimension-six SMEFT operators in the Warsaw basis.

C Observables

We list the observables included in our analysis in Tables 3-6. Table 3 lists observables from Higgs physics and Zjj production, Tables 4 and 5 list observables from the top sector as well as Drell-Yan and dijet+photon data, and Table 6 lists observables from PVE, lepton scattering and flavour.

Table 3: Higgs and electroweak observables included in the fit.

Observables		no. of measurements	References	
Higgs Data		159		
7 and 8 TeV	ATLAS & CMS combination	20	Table 8 of Ref. [95]	
	ATLAS & CMS combination $\mu(h \rightarrow \mu\mu)$	1	Table 13 of Ref. [95]	
Run-I data	ATLAS $\mu(h \rightarrow Z\gamma)$	1	Figure 1 of Ref. [96]	
13 TeV ATLAS Run-II data	$\mu(h \rightarrow Z\gamma)$ at 139 fb ⁻¹	1	[97]	
	$\mu(h \rightarrow \mu\mu)$ at 139 fb ⁻¹	1	[98]	
	$\mu(h \rightarrow \tau\tau)$ at 139 fb ⁻¹	4	Figure 14 of Ref. [99]	
	$\mu(h \rightarrow bb)$ in VBF and ttH at 139 fb ⁻¹	1+1	[100, 101]	
	STXS $h \rightarrow \gamma\gamma/ZZ/b\bar{b}$ at 139 fb ⁻¹	42	Figures 1 and 2 of Ref. [102]	
	STXS $h \rightarrow WW$ in ggF, VBF at 139 fb ⁻¹	11	Figures 12 and 14 of Ref. [103]	
	di-Higgs $\mu_{HH}^{b\bar{b}b\bar{b}}, \mu_{HH}^{b\bar{b}\tau\bar{\tau}}, \mu_{HH}^{b\bar{b}\gamma\gamma}$	3	[104–106]	
13 TeV CMS Run-II data	$\mu(h \rightarrow b\bar{b})$ in Vh at 35.9/41.5 fb ⁻¹	2	entries from Table 4 of Ref. [107]	
	$\mu(h \rightarrow WW)$ in ggF at 137 fb ⁻¹	1	[108]	
	$\mu(h \rightarrow \mu\mu)$ at 137 fb ⁻¹	4	Figure 11 of Ref. [109]	
	$\mu(h \rightarrow \tau\tau/WW)$ in $t\bar{t}h$ at 137 fb ⁻¹	3	Figure 14 of Ref. [110]	
	STXS $h \rightarrow WW$ at 137 fb ⁻¹ in Vh	4	Table 9 of Ref. [111]	
	STXS $h \rightarrow \tau\tau$ at 137 fb ⁻¹	11	Figures 11/12 of Ref. [112]	
	STXS $h \rightarrow \gamma\gamma$ at 137 fb ⁻¹	27	Table 13 and Figure 21 of Ref. [113]	
	STXS $h \rightarrow ZZ$ at 137 fb ⁻¹	18	Table 6 and Figure 15 of Ref. [114]	
		di-Higgs $\mu_{HH}^{b\bar{b}b\bar{b}}, \mu_{HH}^{b\bar{b}\tau\bar{\tau}}, \mu_{HH}^{b\bar{b}\gamma\gamma}$	3	[115–117]
		ATLAS Zjj 13 TeV $\Delta\phi_{jj}$ at 139 fb ⁻¹	12	Figure 7(d) of Ref. [118]

Table 4: Top physics observables from Tevatron and LHC Run I included in the fit.

Observables		no. of meas.	References
Top Data from Tevatron and LHC Run I		82	
Tevatron	forward-backward asymmetry $A_{FB}(m_{t\bar{t}})$ for $t\bar{t}$ production	4	[119]
ATLAS & CMS	charge asymmetry $A_C(m_{t\bar{t}})$ for $t\bar{t}$ production in the ℓ +jets channel.	6	[120]
	W -boson helicity fractions in top decay	3	[121]
ATLAS	charge asymmetry $A_C(m_{t\bar{t}})$ for $t\bar{t}$ production in the dilepton channel	1	[122]
	$\sigma_{t\bar{t}W}, \sigma_{t\bar{t}Z}$	2	[123]
	$\frac{d\sigma}{dp_t^T}, \frac{d\sigma}{d y_{t\bar{t}} }$ for t -channel single-top production	4 + 5	[124]
	σ_{tW} in the single lepton channel	1	[125]
	σ_{tW} in the dilepton channel	1	[126]
	s -channel single-top cross section	1	[127]
	$\frac{d\sigma}{dm_{t\bar{t}}}$ for $t\bar{t}$ production in the dilepton channel	6	[128]
	$\frac{d\sigma}{dp_t^T}$ for $t\bar{t}$ production in the ℓ +jets channel	8	[129]
CMS	$\sigma_{t\bar{t}\gamma}$ in the ℓ + jets channel.	1	[130]
	charge asymmetry $A_C(m_{t\bar{t}})$ for $t\bar{t}$ production in the dilepton channel.	3	[131]
	$\sigma_{t\bar{t}W}, \sigma_{t\bar{t}Z}$	2	[130]
	$\sigma_{t\bar{t}\gamma}$ in the ℓ + jets channel.	1	[132]
	s -channel single-top cross section	1	[133]
	$\frac{d\sigma}{dp_{t+\bar{t}}^T}$ of t -channel single-top production	6	[134]
	t -channel single-top and anti-top cross sections R_t .	1	[135]
	σ_{tW}	1	[136]
	$\frac{d\sigma}{dm_{t\bar{t}}dy_{t\bar{t}}}$ for $t\bar{t}$ production in the dilepton channel	16	[137, 138]
	$\frac{d\sigma}{dp_t^T}$ for $t\bar{t}$ production in the ℓ +jets channel	8	[139, 140]

Table 5: Top physics observables from LHC Run II as well as data from Drell-Yan and dijet+photon production included in the analysis.

Observables		no. of meas.	References
Top Data from LHC Run II		55	
ATLAS	σ_{tW}	1	[141]
	σ_{tZ}	1	[142]
	$\sigma_{t+\bar{t}}, R_t$ for t -channel single-top and anti-top cross sections	1+1	[143]
	charge asymmetry $A_C(m_{t\bar{t}})$ for $t\bar{t}$ production	5	[144]
	$\sigma_{t\bar{t}W}, \sigma_{t\bar{t}Z}$	2	[145]
	$\frac{d\sigma}{dp_T^\gamma}$ for $t\bar{t}\gamma$ production	11	[146]
CMS	σ_{tW}	1	[147]
	σ_{tZ} in the $Z \rightarrow \ell^+\ell^-$ channel	1	[148]
	$\frac{d\sigma}{dp_{t+\bar{t}}^T}$ and $R_t(p_{t+\bar{t}}^T)$ for t -channel single-top quark production	5 + 5	[149]
	$\frac{d\sigma}{dm_{t\bar{t}}}$ for $t\bar{t}$ production in the dilepton channel	6	[150]
	$\frac{d\sigma}{dm_{t\bar{t}}}$ for $t\bar{t}$ production in the ℓ +jets channel	15	[151]
	$\sigma_{t\bar{t}W}$	1	[152]
	$\frac{d\sigma}{dp_Z^T}$ for $t\bar{t}Z$ production	4	[153]
Drell-Yan		109	
13 TeV	CMS e^+e^-, m_{ee}	61 (up to 3 TeV)	Figure 2 of [154]
	CMS $\mu^+\mu^-, m_{\mu\mu}$	34 (up to 3 TeV)	Figure 2 of [154]
	ATLAS $\tau^+\tau^-, m_T^{\text{tot}}$	14 (up to 3 TeV)	Figure 1 of [155]
Dijets+photon		26	
13 TeV	ATLAS $\frac{dN_{\text{ext}}}{dm_{jj}}$ for $pp \rightarrow jj\gamma + X$	26 (from 500 GeV)	Figure 1 of [74]

Table 6: EWPO, PVE, lepton scattering and flavour observables included in the fit.

Observables		no. of measurements	References
Electroweak Precision Observables (EWPO)		13	Ref. [48]
PVE and lepton scattering		163	
PVE	Q_W^{Cs}	1	[58]
	Q_W^{P}	1	[59]
	$A_{1,2}^{\text{PVDIS}}$	2	[60]
	SAMPLE	1	[61]
lepton scattering	$\nu_\mu \nu_\mu ee$	2	[58]
	P_τ, A_P	2	[62]
	g_{AV}^{ee} in $e^- e^- \rightarrow e^- e^-$	1	[58]
	$A_{\text{FB}}^{\mu,\tau}$ in $e^+ e^- \rightarrow l^+ l^-$	24	[49, 63]
	$\sigma_{\mu,\tau}$ in $e^+ e^- \rightarrow l^+ l^-$	24	[49, 63]
	$\frac{d\sigma(ee)}{d\cos\theta}$ in $e^+ e^- \rightarrow l^+ l^-$	105	[49, 63]
Flavour		37	
Differential BR($B \rightarrow K\mu\mu$) (from 14 GeV)		3	[156]
Differential BR($B \rightarrow K^*\mu\mu$) (from 14 GeV)		3	[157]
Differential BR($\Lambda_b \rightarrow \Lambda\mu\mu$) (from 15 GeV)		1	[158]
BR($B \rightarrow X_s\mu\mu, \mu\mu, X_s\gamma, K^*\gamma, K^{(*)}\bar{\nu}\nu$)		5	[159–163]
BR($B_s \rightarrow \mu\mu, \phi\gamma$)		2	[160, 164]
BR($K^+ \rightarrow \mu^+\nu_\mu$)		1	[94]
R_K and R_K^*		4	[165]
B meson mixing observables		2	[166]
Angular observables in $B \rightarrow K^*\mu\mu$ and $\Lambda_b \rightarrow \Lambda\mu\mu$ (from 15 GeV)		16	[158, 167]

D Numerical results

We present the correlation matrix of our global analysis including partial NLO SMEFT predictions in Figure 14. Numerical values for the fit results of the single-parameter fit as well as the global fit can be found in Table 7.

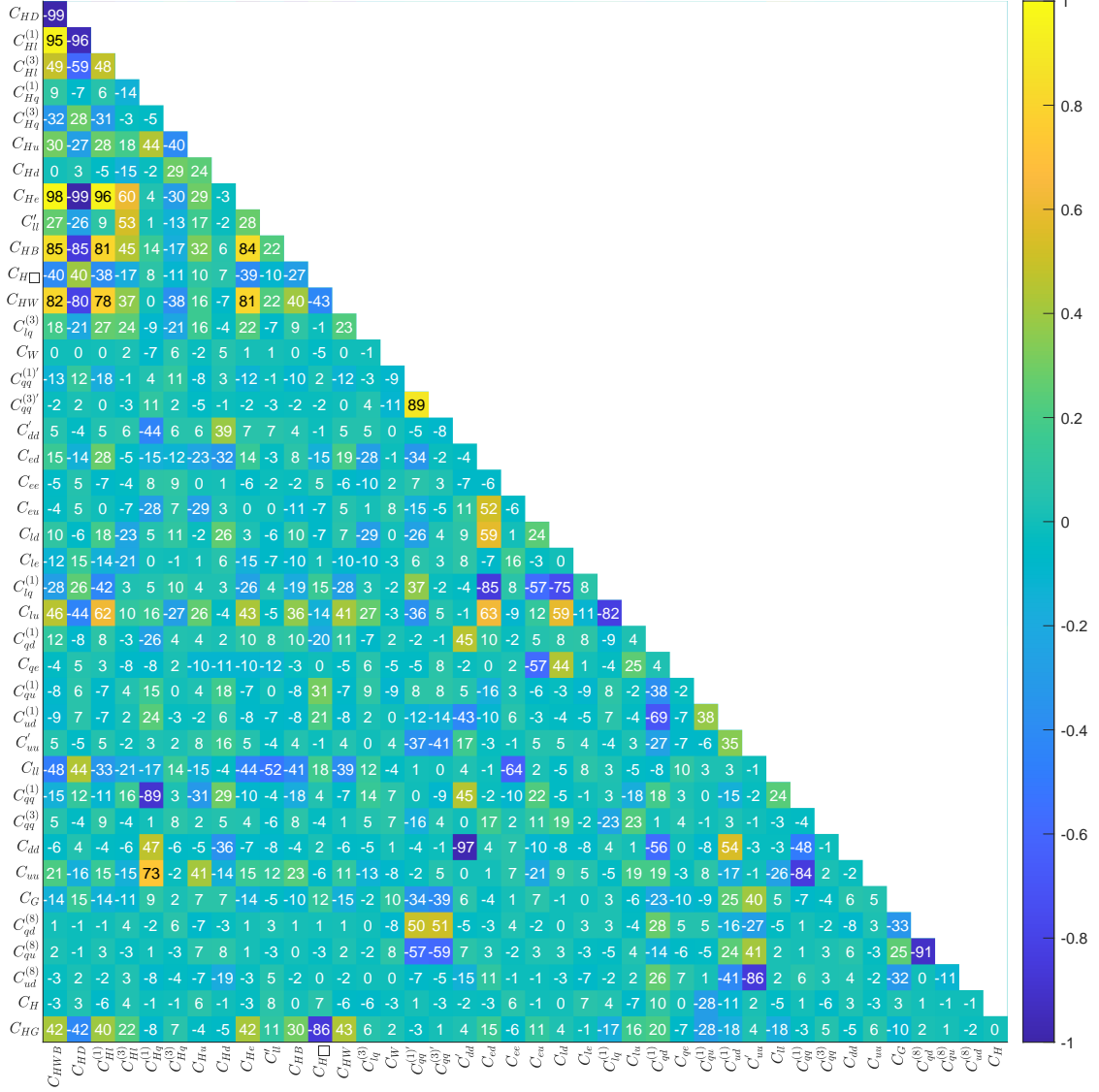


Figure 14: Correlation matrix of the global analysis including partial NLO SMEFT predictions. The numbers in the matrix correspond to the correlations in percent.

coefficient	LO SMEFT predictions		partial NLO SMEFT predictions	
	single 95%CL limit	global 95%CL limit	single 95%CL limit	global 95%CL limit
C_{HWB}	[-0.004, 0.002]	[-0.12, 0.15]	[-0.004, 0.002]	[-0.1, 0.18]
C_{HD}	[-0.022, 0.003]	[-0.39, 0.26]	[-0.022, 0.003]	[-0.43, 0.23]
$C_{Hl}^{(1)}$	[-0.006, 0.011]	[-0.06, 0.11]	[-0.006, 0.011]	[-0.04, 0.15]
$C_{Hl}^{(3)}$	[-0.01, 0.003]	[-0.049, 0.063]	[-0.01, 0.003]	[-0.062, 0.051]
$C_{Hq}^{(1)}$	[-0.035, 0.014]	[-0.096, 0.055]	[-0.035, 0.014]	[-0.14, 0.23]
$C_{Hq}^{(3)}$	[-0.01, 0.013]	[-0.036, 0.048]	[-0.01, 0.013]	[-0.04, 0.045]
C_{Hu}	[-0.048, 0.04]	[-0.22, 0.12]	[-0.048, 0.04]	[-0.17, 0.22]
C_{Hd}	[-0.094, 0.016]	[-0.65, 0.16]	[-0.094, 0.016]	[-0.56, 0.34]
C_{He}	[-0.012, 0.009]	[-0.14, 0.19]	[-0.012, 0.009]	[-0.13, 0.21]
C'_{ll}	[-0.004, 0.017]	[-0.071, 0.018]	[-0.004, 0.017]	[-0.075, 0.016]
C_{ll}	[-0.011, 0.048]	[-0.0, 0.22]	[-0.011, 0.048]	[-0.01, 0.21]
C_{ee}	[-0.022, 0.04]	[-0.16, 0.02]	[-0.022, 0.04]	[-0.16, 0.01]
C_{le}	[-0.028, 0.027]	[-0.026, 0.039]	[-0.028, 0.027]	[-0.027, 0.039]
C_{HB}	[-0.003, 0.002]	[-0.03, 0.067]	[-0.003, 0.002]	[-0.022, 0.077]
$C_{H\Box}$	[-1.0, -0.2]	[-1.4, 0.3]	[-1.0, -0.2]	[-1.3, 0.5]
C_{HW}	[-0.009, 0.007]	[-0.19, 0.12]	[-0.009, 0.007]	[-0.18, 0.13]
C_H	[-9.5, 7.7]	[-11, 6]	[-9.5, 7.7]	[-13, 4]
C_{HG}	[-0.004, -0.0]	[-0.004, 0.004]	[-0.004, -0.0]	[-0.005, 0.003]
C_G	[-0.36, 0.16]	[-0.44, 0.19]	[-0.36, 0.16]	[-0.53, 0.2]
C_W	[-0.17, 0.36]	[-0.17, 0.36]	[-0.19, 0.34]	[-0.18, 0.36]
$C_{lq}^{(1)}$	[-0.005, 0.018]	[-0.67, 0.08]	[-0.004, 0.019]	[-0.61, 0.12]
$C_{lq}^{(3)}$	[-0.006, 0.002]	[-0.09, 0.11]	[-0.006, 0.002]	[-0.09, 0.11]
C_{ed}	[-0.04, 0.008]	[-0.17, 0.8]	[-0.04, 0.008]	[-0.27, 0.65]
C_{eu}	[-0.005, 0.011]	[-0.29, 0.34]	[-0.005, 0.011]	[-0.35, 0.25]
C_{ld}	[-0.039, 0.043]	[-0.3, 1.8]	[-0.039, 0.043]	[-0.2, 1.9]
C_{lu}	[-0.007, 0.025]	[-0.2, 1.3]	[-0.008, 0.024]	[-0.2, 1.3]
C_{qe}	[-0.016, 0.019]	[-0.13, 0.79]	[-0.016, 0.019]	[-0.12, 0.78]
$C_{qd}^{(1)}$	[-34, 23]	[-1760, 1090]	[-0.3, 1.7]	[-3.0, 5.2]
$C_{qu}^{(1)}$	[-4.9, 7.3]	[-380, 340]	[0.0, 0.6]	[-0.2, 1.8]
$C_{ud}^{(1)}$	[-7.2, 4.7]	[-520, 370]	[-1.8, 0.7]	[-7.4, 3.9]
$C_{qq}^{(1)}$	[-0.13, 0.19]	[-12, 1]	[-0.15, 0.16]	[-6.7, 3.4]
$C_{qq}^{(1)'} $	[-0.039, 0.018]	[-0.07, 0.39]	[-0.039, 0.018]	[-0.06, 0.42]
$C_{qq}^{(3)}$	[-0.021, 0.04]	[-0.01, 0.11]	[-0.021, 0.04]	[-0.01, 0.1]
$C_{qq}^{(3)'} $	[-0.017, 0.029]	[-0.05, 0.35]	[-0.017, 0.029]	[-0.05, 0.38]
C_{uu}	[-0.14, 0.22]	[-2, 15]	[-0.18, 0.17]	[-0.9, 8.8]
C'_{uu}	[-0.15, 0.07]	[-1.8, 0.3]	[-0.15, 0.07]	[-2.3, 0.4]
C_{dd}	[-1.8, 2.7]	[-210, 70]	[-1.9, 2.6]	[-190, 30]
C'_{dd}	[-1.2, 1.8]	[-62, 82]	[-1.2, 1.8]	[-19, 84]
$C_{qd}^{(8)}$	[-0.8, 0.21]	[-3.6, 2.7]	[-0.8, 0.21]	[-3.8, 3.6]
$C_{qu}^{(8)}$	[-0.18, 0.06]	[-0.7, 0.51]	[-0.18, 0.06]	[-0.86, 0.53]
$C_{ud}^{(8)}$	[-0.59, 0.23]	[-4.6, 4.0]	[-0.59, 0.23]	[-4.9, 5.8]

Table 7: Numerical results of the single-parameter and global analyses using purely LO or partial NLO SMEFT predictions. Fit results which do not change between the two setups have been greyed out.

E LEFT Hamiltonians for the relevant flavour observables

We present the relevant Hamiltonians for the flavour violating observables in Table 6 where the corresponding Wilson coefficients are defined at the EW scale. The Hamiltonian for $d_i \rightarrow d_j l^+ l^-$ and $d_i \rightarrow d_j \gamma$ transitions is defined as

$$\mathcal{H}_{\text{eff}}^{ll} \supset \frac{4G_F}{\sqrt{2}} \left[-\frac{1}{(4\pi)^2} V_{td_j}^* V_{td_i} \sum_{i=3}^{10} C_i^{d_i d_j} \mathcal{O}_i^{d_i d_j} + \sum_{q=u,c} V_{qd_j}^* V_{qd_i} (C_1^{d_i d_j} \mathcal{O}_1^{q, d_i d_j} + C_2^{d_i d_j} \mathcal{O}_2^{q, d_i d_j}) \right]. \quad (\text{E.1})$$

The operators of relevance to this analysis given by

$$\begin{aligned} \mathcal{O}_1^{q, d_i d_j} &= (\bar{d}_i^\alpha \gamma_\mu P_L q^\beta) (\bar{q}^\beta \gamma^\mu P_L d_j^\alpha), \\ \mathcal{O}_2^{q, d_i d_j} &= (\bar{d}_i^\alpha \gamma_\mu P_L q^\alpha) (\bar{q}^\beta \gamma^\mu P_L d_j^\beta), \\ \mathcal{O}_7^{d_i d_j} &= e m_{d_i} (\bar{d}_j \sigma^{\mu\nu} P_R d_i) F_{\mu\nu}, \\ \mathcal{O}_8^{d_i d_j} &= g_s m_{d_i} (\bar{d}_j \sigma^{\mu\nu} T^A P_R d_i) G_{\mu\nu}^A, \\ \mathcal{O}_9^{d_i d_j} &= e^2 (\bar{d}_j \gamma^\mu P_L d_i) (\bar{\ell} \gamma_\mu \ell), \\ \mathcal{O}_{10}^{d_i d_j} &= e^2 (\bar{d}_j \gamma^\mu P_L d_i) (\bar{\ell} \gamma_\mu \gamma_5 \ell), \end{aligned} \quad (\text{E.2})$$

where α, β are colour indices. Since our fit is linear in the SMEFT Wilson coefficients, the terms appearing in each observable are given by the interference with the SM. Therefore, we can neglect contributions to flavour observables arising from $\mathcal{O}_{3,4,5,6}$ because the matching of the SM onto these LEFT coefficients gives much smaller values with respect to the remaining operators in Equation (E.1). The LEFT effective Hamiltonian for $d_i \rightarrow d_j \bar{\nu} \nu$ is given by

$$\mathcal{H}_{\text{eff}}^{\nu\nu} \supset -\frac{4G_F}{\sqrt{2}} \frac{1}{(4\pi)^2} \frac{e^2}{\sin^2 \theta_W} V_{td_j}^* V_{td_i} C_L^{d_i d_j} (\bar{d}_j \gamma^\mu P_L d_i) (\bar{\nu}_k \gamma^\mu (1 - \gamma^5) \nu_k). \quad (\text{E.3})$$

The LEFT Hamiltonian relevant for charged-current semileptonic decays $d_i \rightarrow u_j l \bar{\nu}$ is

$$\mathcal{H}_{\text{eff}} = \frac{4G_F V_{u_j d_i}}{\sqrt{2}} C_\pm \sum_l (\bar{l} \gamma_\mu P_L \nu_l) (\bar{u}_i \gamma^\mu P_L d_j) + \text{h.c.} \quad (\text{E.4})$$

This process already exists in the SM and we hence get tree-level contributions to C_\pm . Finally, the LEFT Hamiltonian relevant for meson mixing is

$$\begin{aligned} \mathcal{H}_{\text{eff}}^{\text{mix}} &\supset \frac{G_F^2 m_W^2}{16\pi^2} (\bar{d}_j^\alpha \gamma^\mu P_L d_i^\alpha) (\bar{d}_j^\beta \gamma^\mu P_L d_i^\beta) \\ &\times \left(\lambda_t^2 C_{1,\text{mix}}^{d_i d_j}(x_t) + \lambda_c^2 C_{1,\text{mix}}^{d_i d_j}(x_c) + 2 \lambda_c \lambda_t C_{1,\text{mix}}^{d_i d_j}(x_t, x_c) \right), \end{aligned} \quad (\text{E.5})$$

where α and β are colour indices, $\lambda_k = V_{kd_j}^* V_{kd_i}$ and $x_k = m_k^2/m_W^2$.

References

- [1] W. Buchmuller and D. Wyler, *Effective Lagrangian Analysis of New Interactions and Flavor Conservation*, *Nucl. Phys. B* **268** (1986) 621–653.
- [2] F. Wilczek, *Problem of Strong P and T Invariance in the Presence of Instantons*, *Phys. Rev. Lett.* **40** (1978) 279–282.
- [3] B. Grzadkowski, M. Iskrzynski, M. Misiak and J. Rosiek, *Dimension-Six Terms in the Standard Model Lagrangian*, *JHEP* **10** (2010) 085, [[1008.4884](#)].
- [4] I. Brivio and M. Trott, *The Standard Model as an Effective Field Theory*, *Phys. Rept.* **793** (2019) 1–98, [[1706.08945](#)].
- [5] A. Falkowski, M. González-Alonso and K. Mimouni, *Compilation of low-energy constraints on 4-fermion operators in the SMEFT*, *JHEP* **08** (2017) 123, [[1706.03783](#)].
- [6] A. Biekötter, T. Corbett and T. Plehn, *The Gauge-Higgs Legacy of the LHC Run II*, *SciPost Phys.* **6** (2019) 064, [[1812.07587](#)].
- [7] S. Kraml, T. Q. Loc, D. T. Nhung and L. D. Ninh, *Constraining new physics from Higgs measurements with Lilith: update to LHC Run 2 results*, *SciPost Phys.* **7** (2019) 052, [[1908.03952](#)].
- [8] S. Dawson, S. Homiller and S. D. Lane, *Putting standard model EFT fits to work*, *Phys. Rev. D* **102** (2020) 055012, [[2007.01296](#)].
- [9] E. d. S. Almeida, A. Alves, O. J. P. Éboli and M. C. Gonzalez-Garcia, *Electroweak legacy of the LHC run II*, *Phys. Rev. D* **105** (2022) 013006, [[2108.04828](#)].
- [10] Anisha, S. Das Bakshi, S. Banerjee, A. Biekötter, J. Chakraborty, S. Kumar Patra et al., *Effective limits on single scalar extensions in the light of recent LHC data*, *Phys. Rev. D* **107** (2023) 055028, [[2111.05876](#)].
- [11] A. Buckley, C. Englert, J. Ferrando, D. J. Miller, L. Moore, M. Russell et al., *Constraining top quark effective theory in the LHC Run II era*, *JHEP* **04** (2016) 015, [[1512.03360](#)].
- [12] D. Barducci et al., *Interpreting top-quark LHC measurements in the standard-model effective field theory*, [1802.07237](#).
- [13] I. Brivio, S. Bruggisser, F. Maltoni, R. Moutafis, T. Plehn, E. Vryonidou et al., *O new physics, where art thou? A global search in the top sector*, *JHEP* **02** (2020) 131, [[1910.03606](#)].
- [14] S. Bißmann, J. Erdmann, C. Grunwald, G. Hiller and K. Kröninger, *Constraining top-quark couplings combining top-quark and B decay observables*, *Eur. Phys. J. C* **80** (2020) 136, [[1909.13632](#)].
- [15] G. Durieux, A. Irlles, V. Miralles, A. Peñuelas, R. Pöschl, M. Perelló et al., *The electro-weak couplings of the top and bottom quarks — Global fit and future prospects*, *JHEP* **12** (2019) 98, [[1907.10619](#)].
- [16] J. Ellis, M. Madigan, K. Mimasu, V. Sanz and T. You, *Top, Higgs, Diboson and Electroweak Fit to the Standard Model Effective Field Theory*, *JHEP* **04** (2021) 279, [[2012.02779](#)].
- [17] SMEFT collaboration, J. J. Ethier, G. Magni, F. Maltoni, L. Mantani, E. R. Nocera, J. Rojo et al., *Combined SMEFT interpretation of Higgs, diboson, and top quark data from the LHC*, *JHEP* **11** (2021) 089, [[2105.00006](#)].

- [18] F. Garosi, D. Marzocca, A. Rodriguez-Sanchez and A. Stanzione, *Indirect constraints on top quark operators from a global SMEFT analysis*, [2310.00047](#).
- [19] E. E. Jenkins, A. V. Manohar and M. Trott, *Renormalization Group Evolution of the Standard Model Dimension Six Operators I: Formalism and lambda Dependence*, *JHEP* **10** (2013) 087, [[1308.2627](#)].
- [20] E. E. Jenkins, A. V. Manohar and M. Trott, *Renormalization Group Evolution of the Standard Model Dimension Six Operators II: Yukawa Dependence*, *JHEP* **01** (2014) 035, [[1310.4838](#)].
- [21] R. Alonso, E. E. Jenkins, A. V. Manohar and M. Trott, *Renormalization Group Evolution of the Standard Model Dimension Six Operators III: Gauge Coupling Dependence and Phenomenology*, *JHEP* **04** (2014) 159, [[1312.2014](#)].
- [22] L. Calibbi and G. Signorelli, *Charged Lepton Flavour Violation: An Experimental and Theoretical Introduction*, *Riv. Nuovo Cim.* **41** (2018) 71–174, [[1709.00294](#)].
- [23] L. Silvestrini and M. Valli, *Model-independent Bounds on the Standard Model Effective Theory from Flavour Physics*, *Phys. Lett. B* **799** (2019) 135062, [[1812.10913](#)].
- [24] D. A. Faroughy, G. Isidori, F. Wilsch and K. Yamamoto, *Flavour symmetries in the SMEFT*, *JHEP* **08** (2020) 166, [[2005.05366](#)].
- [25] A. Greljo, A. Palavrić and A. E. Thomsen, *Adding Flavor to the SMEFT*, *JHEP* **10** (2022) 010, [[2203.09561](#)].
- [26] R. S. Chivukula and H. Georgi, *Composite Technicolor Standard Model*, *Phys. Lett. B* **188** (1987) 99–104.
- [27] L. J. Hall and L. Randall, *Weak scale effective supersymmetry*, *Phys. Rev. Lett.* **65** (1990) 2939–2942.
- [28] G. D’Ambrosio, G. F. Giudice, G. Isidori and A. Strumia, *Minimal flavor violation: An Effective field theory approach*, *Nucl. Phys. B* **645** (2002) 155–187, [[hep-ph/0207036](#)].
- [29] S. Bruggisser, R. Schäfer, D. van Dyk and S. Westhoff, *The Flavor of UV Physics*, *JHEP* **05** (2021) 257, [[2101.07273](#)].
- [30] S. Bruggisser, D. van Dyk and S. Westhoff, *Resolving the flavor structure in the MFV-SMEFT*, *JHEP* **02** (2023) 225, [[2212.02532](#)].
- [31] C. Grunwald, G. Hiller, K. Kröninger and L. Nollen, *More Synergies from Beauty, Top, Z and Drell-Yan Measurements in SMEFT*, [2304.12837](#).
- [32] T. Hurth, S. Renner and W. Shepherd, *Matching for FCNC effects in the flavour-symmetric SMEFT*, *JHEP* **06** (2019) 029, [[1903.00500](#)].
- [33] R. Aoude, T. Hurth, S. Renner and W. Shepherd, *The impact of flavour data on global fits of the MFV SMEFT*, *JHEP* **12** (2020) 113, [[2003.05432](#)].
- [34] A. Greljo and A. Palavrić, *Leading directions in the SMEFT*, *JHEP* **09** (2023) 009, [[2305.08898](#)].
- [35] L. Allwicher, C. Cornella, B. A. Stefanek and G. Isidori, *New Physics in the Third Generation: A Comprehensive SMEFT Analysis and Future Prospects*, [2311.00020](#).
- [36] J. J. Ethier, R. Gomez-Ambrosio, G. Magni and J. Rojo, *SMEFT analysis of vector boson scattering and diboson data from the LHC Run II*, *Eur. Phys. J. C* **81** (2021) 560, [[2101.03180](#)].

- [37] F. Ferreira, B. Fuks, V. Sanz and D. Sengupta, *Probing CP-violating Higgs and gauge-boson couplings in the Standard Model effective field theory*, *Eur. Phys. J. C* **77** (2017) 675, [[1612.01808](#)].
- [38] J. Brehmer, F. Kling, T. Plehn and T. M. P. Tait, *Better Higgs-CP Tests Through Information Geometry*, *Phys. Rev. D* **97** (2018) 095017, [[1712.02350](#)].
- [39] F. U. Bernlochner, C. Englert, C. Hays, K. Lohwasser, H. Mildner, A. Pilkington et al., *Angles on CP-violation in Higgs boson interactions*, *Phys. Lett. B* **790** (2019) 372–379, [[1808.06577](#)].
- [40] C. Englert, P. Galler, A. Pilkington and M. Spannowsky, *Approaching robust EFT limits for CP-violation in the Higgs sector*, *Phys. Rev. D* **99** (2019) 095007, [[1901.05982](#)].
- [41] V. Cirigliano, A. Crivellin, W. Dekens, J. de Vries, M. Hoferichter and E. Mereghetti, *CP Violation in Higgs-Gauge Interactions: From Tabletop Experiments to the LHC*, *Phys. Rev. Lett.* **123** (2019) 051801, [[1903.03625](#)].
- [42] A. Biekötter, R. Gomez-Ambrosio, P. Gregg, F. Krauss and M. Schönherr, *Constraining SMEFT operators with associated $h\gamma$ production in weak boson fusion*, *Phys. Lett. B* **814** (2021) 136079, [[2003.06379](#)].
- [43] A. Biekötter, P. Gregg, F. Krauss and M. Schönherr, *Constraining CP violating operators in charged and neutral triple gauge couplings*, *Phys. Lett. B* **817** (2021) 136311, [[2102.01115](#)].
- [44] S. D. Bakshi, J. Chakraborty, C. Englert, M. Spannowsky and P. Stylianou, *Landscaping CP-violating BSM scenarios*, *Nucl. Phys. B* **975** (2022) 115676, [[2103.15861](#)].
- [45] C. Degrande and J. Touch eque, *A reduced basis for CP violation in SMEFT at colliders and its application to diboson production*, *JHEP* **04** (2022) 032, [[2110.02993](#)].
- [46] A. Bhardwaj, C. Englert, R. Hankache and A. D. Pilkington, *Machine-enhanced CP-asymmetries in the Higgs sector*, *Phys. Lett. B* **832** (2022) 137246, [[2112.05052](#)].
- [47] N. C. Hall, I. Criddle, A. Crossland, C. Englert, P. Forbes, R. Hankache et al., *Machine-enhanced CP-asymmetries in the electroweak sector*, *Phys. Rev. D* **107** (2023) 016008, [[2209.05143](#)].
- [48] ALEPH, DELPHI, L3, OPAL, SLD, LEP ELECTROWEAK WORKING GROUP, SLD ELECTROWEAK GROUP, SLD HEAVY FLAVOUR GROUP collaboration, S. Schael et al., *Precision electroweak measurements on the Z resonance*, *Phys. Rept.* **427** (2006) 257–454, [[hep-ex/0509008](#)].
- [49] ALEPH, DELPHI, L3, OPAL, LEP ELECTROWEAK collaboration, S. Schael et al., *Electroweak Measurements in Electron-Positron Collisions at W-Boson-Pair Energies at LEP*, *Phys. Rept.* **532** (2013) 119–244, [[1302.3415](#)].
- [50] CDF, D0 collaboration, T. E. W. Group, *2012 Update of the Combination of CDF and D0 Results for the Mass of the W Boson*, [1204.0042](#).
- [51] ATLAS collaboration, M. Aaboud et al., *Measurement of the W-boson mass in pp collisions at $\sqrt{s} = 7$ TeV with the ATLAS detector*, *Eur. Phys. J. C* **78** (2018) 110, [[1701.07240](#)].
- [52] PARTICLE DATA GROUP collaboration, P. A. Zyla et al., *Review of Particle Physics*, *PTEP* **2020** (2020) 083C01.
- [53] L. Berthier and M. Trott, *Consistent constraints on the Standard Model Effective Field Theory*, *JHEP* **02** (2016) 069, [[1508.05060](#)].

- [54] L. Berthier and M. Trott, *Towards consistent Electroweak Precision Data constraints in the SMEFT*, *JHEP* **05** (2015) 024, [[1502.02570](#)].
- [55] M. Bjørn and M. Trott, *Interpreting W mass measurements in the SMEFT*, *Phys. Lett. B* **762** (2016) 426–431, [[1606.06502](#)].
- [56] L. Berthier, M. Bjørn and M. Trott, *Incorporating doubly resonant W^\pm data in a global fit of SMEFT parameters to lift flat directions*, *JHEP* **09** (2016) 157, [[1606.06693](#)].
- [57] I. Brivio, T. Corbett and M. Trott, *The Higgs width in the SMEFT*, *JHEP* **10** (2019) 056, [[1906.06949](#)].
- [58] PARTICLE DATA GROUP collaboration, C. Patrignani et al., *Review of Particle Physics*, *Chin. Phys. C* **40** (2016) 100001.
- [59] QWEAK collaboration, D. Androic et al., *First Determination of the Weak Charge of the Proton*, *Phys. Rev. Lett.* **111** (2013) 141803, [[1307.5275](#)].
- [60] PVDIS collaboration, D. Wang et al., *Measurement of parity violation in electron–quark scattering*, *Nature* **506** (2014) 67–70.
- [61] E. J. Beise, M. L. Pitt and D. T. Spayde, *The SAMPLE experiment and weak nucleon structure*, *Prog. Part. Nucl. Phys.* **54** (2005) 289–350, [[nuc1-ex/0412054](#)].
- [62] VENUS collaboration, H. Hanai et al., *Measurement of tau polarization in e^+e^- annihilation at $s^{*(1/2)} = 58\text{-GeV}$* , *Phys. Lett. B* **403** (1997) 155–162, [[hep-ex/9703003](#)].
- [63] LEP, ALEPH, DELPHI, L3, OPAL, LEP ELECTROWEAK WORKING GROUP, SLD ELECTROWEAK GROUP, SLD HEAVY FLAVOR GROUP collaboration, t. S. Electroweak, *A Combination of preliminary electroweak measurements and constraints on the standard model*, [hep-ex/0312023](#).
- [64] A. Falkowski and K. Mimouni, *Model independent constraints on four-lepton operators*, *JHEP* **02** (2016) 086, [[1511.07434](#)].
- [65] L. Allwicher, D. A. Faroughy, F. Jaffredo, O. Sumensari and F. Wilsch, *HighPT: A tool for high- p_T Drell-Yan tails beyond the standard model*, *Comput. Phys. Commun.* **289** (2023) 108749, [[2207.10756](#)].
- [66] D. M. Straub, *flavio: a Python package for flavour and precision phenomenology in the Standard Model and beyond*, [1810.08132](#).
- [67] E. E. Jenkins, A. V. Manohar and P. Stoffer, *Low-Energy Effective Field Theory below the Electroweak Scale: Operators and Matching*, *JHEP* **03** (2018) 016, [[1709.04486](#)].
- [68] E. E. Jenkins, A. V. Manohar and P. Stoffer, *Low-Energy Effective Field Theory below the Electroweak Scale: Anomalous Dimensions*, *JHEP* **01** (2018) 084, [[1711.05270](#)].
- [69] W. Dekens and P. Stoffer, *Low-energy effective field theory below the electroweak scale: matching at one loop*, *JHEP* **10** (2019) 197, [[1908.05295](#)].
- [70] A. Celis, J. Fuentes-Martin, A. Vicente and J. Virto, *DsixTools: The Standard Model Effective Field Theory Toolkit*, *Eur. Phys. J. C* **77** (2017) 405, [[1704.04504](#)].
- [71] J. Fuentes-Martin, P. Ruiz-Femenia, A. Vicente and J. Virto, *DsixTools 2.0: The Effective Field Theory Toolkit*, *Eur. Phys. J. C* **81** (2021) 167, [[2010.16341](#)].
- [72] J. Aebischer, J. Kumar and D. M. Straub, *Wilson: a Python package for the running and matching of Wilson coefficients above and below the electroweak scale*, *Eur. Phys. J. C* **78** (2018) 1026, [[1804.05033](#)].

- [73] E. Keilmann and W. Shepherd, *Dijets at Tevatron Cannot Constrain SMEFT Four-Quark Operators*, *JHEP* **09** (2019) 086, [[1907.13160](#)].
- [74] ATLAS collaboration, M. Aaboud et al., *Search for low-mass resonances decaying into two jets and produced in association with a photon using pp collisions at $\sqrt{s} = 13$ TeV with the ATLAS detector*, *Phys. Lett. B* **795** (2019) 56–75, [[1901.10917](#)].
- [75] J. Alwall, R. Frederix, S. Frixione, V. Hirschi, F. Maltoni, O. Mattelaer et al., *The automated computation of tree-level and next-to-leading order differential cross sections, and their matching to parton shower simulations*, *JHEP* **07** (2014) 079, [[1405.0301](#)].
- [76] T. Sjöstrand, S. Ask, J. R. Christiansen, R. Corke, N. Desai, P. Ilten et al., *An Introduction to PYTHIA 8.2*, *Comput. Phys. Commun.* **191** (2015) 159–177, [[1410.3012](#)].
- [77] A. Buckley, J. Butterworth, L. Lonnblad, D. Grellscheid, H. Hoeth, J. Monk et al., *Rivet user manual*, *Comput. Phys. Commun.* **184** (2013) 2803–2819, [[1003.0694](#)].
- [78] I. Brivio, *SMEFTsim 3.0 — a practical guide*, *JHEP* **04** (2021) 073, [[2012.11343](#)].
- [79] S. Dawson and P. P. Giardino, *Electroweak and QCD corrections to Z and W pole observables in the standard model EFT*, *Phys. Rev. D* **101** (2020) 013001, [[1909.02000](#)].
- [80] S. Dawson and P. P. Giardino, *Flavorful electroweak precision observables in the Standard Model effective field theory*, *Phys. Rev. D* **105** (2022) 073006, [[2201.09887](#)].
- [81] N. P. Hartland, F. Maltoni, E. R. Nocera, J. Rojo, E. Slade, E. Vryonidou et al., *A Monte Carlo global analysis of the Standard Model Effective Field Theory: the top quark sector*, *JHEP* **04** (2019) 100, [[1901.05965](#)].
- [82] Z. Kassabov, M. Madigan, L. Mantani, J. Moore, M. Morales Alvarado, J. Rojo et al., *The top quark legacy of the LHC Run II for PDF and SMEFT analyses*, *JHEP* **05** (2023) 205, [[2303.06159](#)].
- [83] L. Alasfar, J. de Blas and R. Gröber, *Higgs probes of top quark contact interactions and their interplay with the Higgs self-coupling*, *JHEP* **05** (2022) 111, [[2202.02333](#)].
- [84] A. Biekötter, B. D. Pecjak, D. J. Scott and T. Smith, *Electroweak input schemes and universal corrections in SMEFT*, *JHEP* **07** (2023) 115, [[2305.03763](#)].
- [85] G. Degrandi, P. P. Giardino, F. Maltoni and D. Pagani, *Probing the Higgs self coupling via single Higgs production at the LHC*, *JHEP* **12** (2016) 080, [[1607.04251](#)].
- [86] G. Degrandi and M. Vitti, *The effect of an anomalous Higgs trilinear self-coupling on the $h \rightarrow \gamma Z$ decay*, *Eur. Phys. J. C* **80** (2020) 307, [[1912.06429](#)].
- [87] V. Cirigliano, W. Dekens, J. de Vries, E. Mereghetti and T. Tong, *Beta-decay implications for the W-boson mass anomaly*, *Phys. Rev. D* **106** (2022) 075001, [[2204.08440](#)].
- [88] M. Thomas Arun, K. Deka and T. Srivastava, *Constraining SMEFT BSM scenarios with EWPO and Δ_{CKM}* , [2301.09273](#).
- [89] V. Cirigliano, W. Dekens, J. de Vries, E. Mereghetti and T. Tong, *Anomalies in global SMEFT analyses: a case study of first-row CKM unitarity*, [2311.00021](#).
- [90] M. González-Alonso and J. Martin Camalich, *Global Effective-Field-Theory analysis of New-Physics effects in (semi)leptonic kaon decays*, *JHEP* **12** (2016) 052, [[1605.07114](#)].
- [91] A. Falkowski, M. González-Alonso and O. Naviliat-Cuncic, *Comprehensive analysis of beta decays within and beyond the Standard Model*, *JHEP* **04** (2021) 126, [[2010.13797](#)].

- [92] R. Boughezal, F. Petriello and D. Wiegand, *Disentangling Standard Model EFT operators with future low-energy parity-violating electron scattering experiments*, *Phys. Rev. D* **104** (2021) 016005, [[2104.03979](#)].
- [93] R. Aoude, F. Maltoni, O. Mattelaer, C. Severi and E. Vryonidou, *Renormalisation group effects on SMEFT interpretations of LHC data*, *JHEP* **09** (2023) 191, [[2212.05067](#)].
- [94] PARTICLE DATA GROUP collaboration, R. L. Workman et al., *Review of Particle Physics*, *PTEP* **2022** (2022) 083C01.
- [95] ATLAS, CMS collaboration, G. Aad et al., *Measurements of the Higgs boson production and decay rates and constraints on its couplings from a combined ATLAS and CMS analysis of the LHC pp collision data at $\sqrt{s} = 7$ and 8 TeV*, *JHEP* **08** (2016) 045, [[1606.02266](#)].
- [96] ATLAS collaboration, G. Aad et al., *Measurements of the Higgs boson production and decay rates and coupling strengths using pp collision data at $\sqrt{s} = 7$ and 8 TeV in the ATLAS experiment*, *Eur. Phys. J. C* **76** (2016) 6, [[1507.04548](#)].
- [97] ATLAS collaboration, G. Aad et al., *A search for the $Z\gamma$ decay mode of the Higgs boson in pp collisions at $\sqrt{s} = 13$ TeV with the ATLAS detector*, *Phys. Lett. B* **809** (2020) 135754, [[2005.05382](#)].
- [98] ATLAS collaboration, G. Aad et al., *A search for the dimuon decay of the Standard Model Higgs boson with the ATLAS detector*, *Phys. Lett. B* **812** (2021) 135980, [[2007.07830](#)].
- [99] ATLAS COLLABORATION collaboration, *Measurements of Higgs boson production cross-sections in the $H \rightarrow \tau^+\tau^-$ decay channel in pp collisions at $\sqrt{s} = 13$ TeV with the ATLAS detector*, tech. rep., CERN, Geneva, Aug, 2021.
- [100] ATLAS collaboration, G. Aad et al., *Measurements of Higgs bosons decaying to bottom quarks from vector boson fusion production with the ATLAS experiment at $\sqrt{s} = 13$ TeV*, *Eur. Phys. J. C* **81** (2021) 537, [[2011.08280](#)].
- [101] ATLAS collaboration, *Measurement of the Higgs boson decaying to b-quarks produced in association with a top-quark pair in pp collisions at $\sqrt{s} = 13$ TeV with the ATLAS detector*, *ATLAS-CONF-2020-058* (11, 2020) .
- [102] ATLAS collaboration, *Interpretations of the combined measurement of Higgs boson production and decay*, *ATLAS-CONF-2020-053* (10, 2020) .
- [103] ATLAS collaboration, *Measurements of gluon fusion and vector-boson-fusion production of the Higgs boson in $H \rightarrow WW^* \rightarrow e\nu\mu\nu$ decays using pp collisions at $\sqrt{s} = 13$ TeV with the ATLAS detector*, *ATLAS-CONF-2021-014* (3, 2021) .
- [104] ATLAS collaboration, M. Aaboud et al., *Search for Higgs boson pair production in the $\gamma\gamma b\bar{b}$ final state with 13 TeV pp collision data collected by the ATLAS experiment*, *JHEP* **11** (2018) 040, [[1807.04873](#)].
- [105] ATLAS collaboration, M. Aaboud et al., *Search for pair production of Higgs bosons in the $b\bar{b}b\bar{b}$ final state using proton-proton collisions at $\sqrt{s} = 13$ TeV with the ATLAS detector*, *JHEP* **01** (2019) 030, [[1804.06174](#)].
- [106] ATLAS collaboration, M. Aaboud et al., *Search for resonant and non-resonant Higgs boson pair production in the $b\bar{b}\tau^+\tau^-$ decay channel in pp collisions at $\sqrt{s} = 13$ TeV with the ATLAS detector*, *Phys. Rev. Lett.* **121** (2018) 191801, [[1808.00336](#)].
- [107] CMS collaboration, *Combined Higgs boson production and decay measurements with up to 137 fb⁻¹ of proton-proton collision data at $\sqrt{s} = 13$ TeV*, *CMS-PAS-HIG-19-005* (2020) .

- [108] CMS collaboration, A. M. Sirunyan et al., *Measurement of the inclusive and differential Higgs boson production cross sections in the leptonic WW decay mode at $\sqrt{s} = 13$ TeV*, *JHEP* **03** (2021) 003, [[2007.01984](#)].
- [109] CMS collaboration, A. M. Sirunyan et al., *Evidence for Higgs boson decay to a pair of muons*, *JHEP* **01** (2021) 148, [[2009.04363](#)].
- [110] CMS collaboration, A. M. Sirunyan et al., *Measurement of the Higgs boson production rate in association with top quarks in final states with electrons, muons, and hadronically decaying tau leptons at $\sqrt{s} = 13$ TeV*, *Eur. Phys. J. C* **81** (2021) 378, [[2011.03652](#)].
- [111] CMS collaboration, *Measurement of Higgs boson production in association with a W or Z boson in the $H \rightarrow WW$ decay channel*, *CMS-PAS-HIG-19-017* (2021) .
- [112] CMS collaboration, *Measurement of Higgs boson production in the decay channel with a pair of τ leptons*, *CMS-PAS-HIG-19-010* (2020) .
- [113] CMS collaboration, A. M. Sirunyan et al., *Measurements of Higgs boson production cross sections and couplings in the diphoton decay channel at $\sqrt{s} = 13$ TeV*, *JHEP* **07** (2021) 027, [[2103.06956](#)].
- [114] CMS collaboration, A. M. Sirunyan et al., *Measurements of production cross sections of the Higgs boson in the four-lepton final state in proton–proton collisions at $\sqrt{s} = 13$ TeV*, *Eur. Phys. J. C* **81** (2021) 488, [[2103.04956](#)].
- [115] CMS collaboration, A. M. Sirunyan et al., *Search for nonresonant Higgs boson pair production in final states with two bottom quarks and two photons in proton-proton collisions at $\sqrt{s} = 13$ TeV*, *JHEP* **03** (2021) 257, [[2011.12373](#)].
- [116] CMS collaboration, *Search for Higgs boson pair production in the four b quark final state*, *CMS-PAS-HIG-20-005* (2021) .
- [117] CMS collaboration, A. M. Sirunyan et al., *Search for Higgs boson pair production in events with two bottom quarks and two tau leptons in proton–proton collisions at $\sqrt{s} = 13$ TeV*, *Phys. Lett. B* **778** (2018) 101–127, [[1707.02909](#)].
- [118] ATLAS collaboration, G. Aad et al., *Differential cross-section measurements for the electroweak production of dijets in association with a Z boson in proton–proton collisions at ATLAS*, *Eur. Phys. J. C* **81** (2021) 163, [[2006.15458](#)].
- [119] CDF, D0 collaboration, T. A. Aaltonen et al., *Combined Forward-Backward Asymmetry Measurements in Top-Antitop Quark Production at the Tevatron*, *Phys. Rev. Lett.* **120** (2018) 042001, [[1709.04894](#)].
- [120] ATLAS, CMS collaboration, M. Aaboud et al., *Combination of inclusive and differential $t\bar{t}$ charge asymmetry measurements using ATLAS and CMS data at $\sqrt{s} = 7$ and 8 TeV*, *JHEP* **04** (2018) 033, [[1709.05327](#)].
- [121] CMS, ATLAS collaboration, G. Aad et al., *Combination of the W boson polarization measurements in top quark decays using ATLAS and CMS data at $\sqrt{s} = 8$ TeV*, *JHEP* **08** (2020) 051, [[2005.03799](#)].
- [122] ATLAS collaboration, G. Aad et al., *Measurements of the charge asymmetry in top-quark pair production in the dilepton final state at $\sqrt{s} = 8$ TeV with the ATLAS detector*, *Phys. Rev. D* **94** (2016) 032006, [[1604.05538](#)].
- [123] ATLAS collaboration, G. Aad et al., *Measurement of the $t\bar{t}W$ and $t\bar{t}Z$ production cross*

- sections in pp collisions at $\sqrt{s} = 8$ TeV with the ATLAS detector, *JHEP* **11** (2015) 172, [[1509.05276](#)].
- [124] ATLAS collaboration, M. Aaboud et al., *Fiducial, total and differential cross-section measurements of t -channel single top-quark production in pp collisions at 8 TeV using data collected by the ATLAS detector*, *Eur. Phys. J. C* **77** (2017) 531, [[1702.02859](#)].
- [125] ATLAS collaboration, G. Aad et al., *Measurement of single top-quark production in association with a W boson in the single-lepton channel at $\sqrt{s} = 8$ TeV with the ATLAS detector*, *Eur. Phys. J. C* **81** (2021) 720, [[2007.01554](#)].
- [126] ATLAS collaboration, G. Aad et al., *Measurement of the production cross-section of a single top quark in association with a W boson at 8 TeV with the ATLAS experiment*, *JHEP* **01** (2016) 064, [[1510.03752](#)].
- [127] ATLAS collaboration, G. Aad et al., *Evidence for single top-quark production in the s -channel in proton-proton collisions at $\sqrt{s} = 8$ TeV with the ATLAS detector using the Matrix Element Method*, *Phys. Lett. B* **756** (2016) 228–246, [[1511.05980](#)].
- [128] ATLAS collaboration, M. Aaboud et al., *Measurement of top quark pair differential cross-sections in the dilepton channel in pp collisions at $\sqrt{s} = 7$ and 8 TeV with ATLAS*, *Phys. Rev. D* **94** (2016) 092003, [[1607.07281](#)].
- [129] ATLAS collaboration, G. Aad et al., *Measurements of top-quark pair differential cross-sections in the lepton+jets channel in pp collisions at $\sqrt{s} = 8$ TeV using the ATLAS detector*, *Eur. Phys. J. C* **76** (2016) 538, [[1511.04716](#)].
- [130] CMS collaboration, V. Khachatryan et al., *Observation of top quark pairs produced in association with a vector boson in pp collisions at $\sqrt{s} = 8$ TeV*, *JHEP* **01** (2016) 096, [[1510.01131](#)].
- [131] CMS collaboration, V. Khachatryan et al., *Measurements of $t\bar{t}$ charge asymmetry using dilepton final states in pp collisions at $\sqrt{s} = 8$ TeV*, *Phys. Lett. B* **760** (2016) 365–386, [[1603.06221](#)].
- [132] CMS collaboration, A. M. Sirunyan et al., *Measurement of the semileptonic $t\bar{t} + \gamma$ production cross section in pp collisions at $\sqrt{s} = 8$ TeV*, *JHEP* **10** (2017) 006, [[1706.08128](#)].
- [133] CMS collaboration, V. Khachatryan et al., *Search for s channel single top quark production in pp collisions at $\sqrt{s} = 7$ and 8 TeV*, *JHEP* **09** (2016) 027, [[1603.02555](#)].
- [134] CMS collaboration, *Single top t -channel differential cross section at 8 TeV*, *CMS-PAS-TOP-14-004* (2014) .
- [135] CMS collaboration, V. Khachatryan et al., *Measurement of the t -channel single-top-quark production cross section and of the $|V_{tb}|$ CKM matrix element in pp collisions at $\sqrt{s} = 8$ TeV*, *JHEP* **06** (2014) 090, [[1403.7366](#)].
- [136] CMS collaboration, S. Chatrchyan et al., *Observation of the associated production of a single top quark and a W boson in pp collisions at $\sqrt{s} = 8$ TeV*, *Phys. Rev. Lett.* **112** (2014) 231802, [[1401.2942](#)].
- [137] CMS collaboration, A. M. Sirunyan et al., *Measurement of double-differential cross sections for top quark pair production in pp collisions at $\sqrt{s} = 8$ TeV and impact on parton distribution functions*, *Eur. Phys. J. C* **77** (2017) 459, [[1703.01630](#)].

- [138] CMS collaboration, S. Chatrchyan et al., *Measurement of the $t\bar{t}$ production cross section in the dilepton channel in pp collisions at $\sqrt{s} = 8$ TeV*, *JHEP* **02** (2014) 024, [[1312.7582](#)].
- [139] CMS collaboration, V. Khachatryan et al., *Measurement of the differential cross section for top quark pair production in pp collisions at $\sqrt{s} = 8$ TeV*, *Eur. Phys. J. C* **75** (2015) 542, [[1505.04480](#)].
- [140] CMS collaboration, V. Khachatryan et al., *Measurements of the $t\bar{t}$ production cross section in lepton+jets final states in pp collisions at 8 TeV and ratio of 8 to 7 TeV cross sections*, *Eur. Phys. J. C* **77** (2017) 15, [[1602.09024](#)].
- [141] ATLAS collaboration, M. Aaboud et al., *Measurement of the cross-section for producing a W boson in association with a single top quark in pp collisions at $\sqrt{s} = 13$ TeV with ATLAS*, *JHEP* **01** (2018) 063, [[1612.07231](#)].
- [142] ATLAS collaboration, M. Aaboud et al., *Measurement of the production cross-section of a single top quark in association with a Z boson in proton-proton collisions at 13 TeV with the ATLAS detector*, *Phys. Lett. B* **780** (2018) 557–577, [[1710.03659](#)].
- [143] ATLAS collaboration, M. Aaboud et al., *Measurement of the inclusive cross-sections of single top-quark and top-antiquark t-channel production in pp collisions at $\sqrt{s} = 13$ TeV with the ATLAS detector*, *JHEP* **04** (2017) 086, [[1609.03920](#)].
- [144] ATLAS collaboration, *Inclusive and differential measurement of the charge asymmetry in $t\bar{t}$ events at 13 TeV with the ATLAS detector*, ATLAS-CONF-2019-026 (7, 2019) .
- [145] ATLAS collaboration, M. Aaboud et al., *Measurement of the $t\bar{t}Z$ and $t\bar{t}W$ cross sections in proton-proton collisions at $\sqrt{s} = 13$ TeV with the ATLAS detector*, *Phys. Rev. D* **99** (2019) 072009, [[1901.03584](#)].
- [146] ATLAS collaboration, G. Aad et al., *Measurements of inclusive and differential cross-sections of combined $t\bar{t}\gamma$ and $tW\gamma$ production in the $e\mu$ channel at 13 TeV with the ATLAS detector*, *JHEP* **09** (2020) 049, [[2007.06946](#)].
- [147] CMS collaboration, A. M. Sirunyan et al., *Measurement of the production cross section for single top quarks in association with W bosons in proton-proton collisions at $\sqrt{s} = 13$ TeV*, *JHEP* **10** (2018) 117, [[1805.07399](#)].
- [148] CMS collaboration, A. M. Sirunyan et al., *Observation of Single Top Quark Production in Association with a Z Boson in Proton-Proton Collisions at $\sqrt{s} = 13$ TeV*, *Phys. Rev. Lett.* **122** (2019) 132003, [[1812.05900](#)].
- [149] CMS collaboration, A. M. Sirunyan et al., *Measurement of differential cross sections and charge ratios for t-channel single top quark production in proton-proton collisions at $\sqrt{s} = 13$ TeV*, *Eur. Phys. J. C* **80** (2020) 370, [[1907.08330](#)].
- [150] CMS collaboration, A. M. Sirunyan et al., *Measurement of the $t\bar{t}$ production cross section, the top quark mass, and the strong coupling constant using dilepton events in pp collisions at $\sqrt{s} = 13$ TeV*, *Eur. Phys. J. C* **79** (2019) 368, [[1812.10505](#)].
- [151] CMS collaboration, *Measurement of differential $t\bar{t}$ production cross sections in the full kinematic range using lepton+jets events from pp collisions at $\sqrt{s} = 13$ TeV*, CMS-PAS-TOP-20-001 (2021) .
- [152] CMS collaboration, A. M. Sirunyan et al., *Measurement of the cross section for top quark pair production in association with a W or Z boson in proton-proton collisions at $\sqrt{s} = 13$ TeV*, *JHEP* **08** (2018) 011, [[1711.02547](#)].

- [153] CMS collaboration, A. M. Sirunyan et al., *Measurement of top quark pair production in association with a Z boson in proton-proton collisions at $\sqrt{s} = 13$ TeV*, *JHEP* **03** (2020) 056, [[1907.11270](#)].
- [154] CMS collaboration, A. M. Sirunyan et al., *Search for resonant and nonresonant new phenomena in high-mass dilepton final states at $\sqrt{s} = 13$ TeV*, *JHEP* **07** (2021) 208, [[2103.02708](#)].
- [155] ATLAS collaboration, G. Aad et al., *Search for heavy Higgs bosons decaying into two tau leptons with the ATLAS detector using pp collisions at $\sqrt{s} = 13$ TeV*, *Phys. Rev. Lett.* **125** (2020) 051801, [[2002.12223](#)].
- [156] LHCb collaboration, R. Aaij et al., *Differential branching fractions and isospin asymmetries of $B \rightarrow K^{(*)}\mu^+\mu^-$ decays*, *JHEP* **06** (2014) 133, [[1403.8044](#)].
- [157] CMS collaboration, V. Khachatryan et al., *Angular analysis of the decay $B^0 \rightarrow K^{*0}\mu^+\mu^-$ from pp collisions at $\sqrt{s} = 8$ TeV*, *Phys. Lett. B* **753** (2016) 424–448, [[1507.08126](#)].
- [158] LHCb collaboration, R. Aaij et al., *Differential branching fraction and angular analysis of $\Lambda_b^0 \rightarrow \Lambda\mu^+\mu^-$ decays*, *JHEP* **06** (2015) 115, [[1503.07138](#)].
- [159] BABAR collaboration, J. P. Lees et al., *Measurement of the $B \rightarrow X_s l^+ l^-$ branching fraction and search for direct CP violation from a sum of exclusive final states*, *Phys. Rev. Lett.* **112** (2014) 211802, [[1312.5364](#)].
- [160] A. Greljo, J. Salko, A. Smolkovič and P. Stangl, *Rare b decays meet high-mass Drell-Yan*, *JHEP* **05** (2023) 087, [[2212.10497](#)].
- [161] M. Misiak and M. Steinhauser, *Weak radiative decays of the B meson and bounds on M_{H^\pm} in the Two-Higgs-Doublet Model*, *Eur. Phys. J. C* **77** (2017) 201, [[1702.04571](#)].
- [162] HFLAV collaboration, Y. Amhis et al., *Averages of b-hadron, c-hadron, and τ -lepton properties as of summer 2014*, [1412.7515](#).
- [163] BABAR collaboration, J. P. Lees et al., *Search for $B \rightarrow K^{(*)}\nu\bar{\nu}$ and invisible quarkonium decays*, *Phys. Rev. D* **87** (2013) 112005, [[1303.7465](#)].
- [164] BELLE collaboration, D. Dutta et al., *Search for $B_s^0 \rightarrow \gamma\gamma$ and a measurement of the branching fraction for $B_s^0 \rightarrow \phi\gamma$* , *Phys. Rev. D* **91** (2015) 011101, [[1411.7771](#)].
- [165] LHCb collaboration, . $\rightarrow K + + -$ et al., *Measurement of lepton universality parameters in $B^+ \rightarrow K^+ \ell^+ \ell^-$ and $B^0 \rightarrow K^{*0} \ell^+ \ell^-$ decays*, *Phys. Rev. D* **108** (2023) 032002, [[2212.09153](#)].
- [166] HFLAV collaboration, Y. Amhis et al., *Averages of b-hadron, c-hadron, and τ -lepton properties as of summer 2016*, *Eur. Phys. J. C* **77** (2017) 895, [[1612.07233](#)].
- [167] LHCb collaboration, R. Aaij et al., *Measurement of CP-Averaged Observables in the $B^0 \rightarrow K^{*0}\mu^+\mu^-$ Decay*, *Phys. Rev. Lett.* **125** (2020) 011802, [[2003.04831](#)].